

bradscholars

Vibro-acoustic products from re-cycled raw materials using a cold extrusion process. A continuous cold extrusion process has been developed to tailor a porous structure from polymeric waste, so that the final material possesses particular vibro-acoustic properties.

Item Type	Thesis
Authors	Khan, Amir
Rights	
The University of Bradford theses are licenced under a Creative Commons Licence.
Download date	2026-04-21 23:46:30
Link to Item	http://hdl.handle.net/10454/4289

Chapter 4

Acoustical Properties of Porous Media and Characterisation Methods

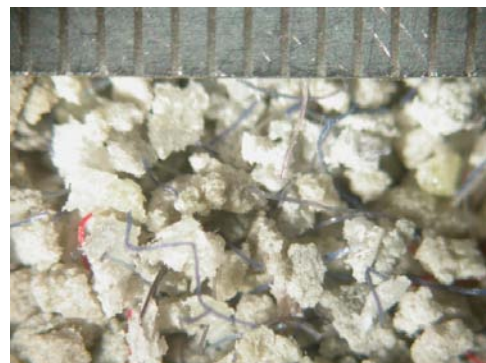
4.1 Introduction

The range of porous media used for acoustic purposes is vast and typical examples are shown in Figure 4.1. So there is a vast range of models which are available to predict their acoustical properties. There are three distinct types of porous media: (i) rigid-frame; (ii) elastic frame and (iii) limp.

This chapter focuses on modelling and characterisation of the rigid-frame porous media and its aim is to discuss critically some of the existing modelling tools which are particularly suitable to describe the acoustical behaviour of the developed material samples. The choice of modelling tools presented in this chapter is by no means complete. The choice is mainly based on the accuracy, simplicity and on general popularity of a particular model.



Reticulated polyurethane foam



Unconsolidated recycled granular and fibre mix

Figure 4.1: Examples of acoustic porous media

The progressive requirement for acoustic materials sustainability from the environmental and economical points of view represents the “driving force” for the development of new poro-elastic materials from industrial and domestic polymeric waste. Traditional solutions based on virgin materials can be replaced if the alternative sustainable products offer equivalent or superior acoustic performance. The success of this work depends heavily on our understanding of acoustic wave propagation in the heterogeneous porous medium and on the availability of accurate prediction tools for engineering optimisation.

4.2 Comparison of modelling approaches for highly heterogeneous porous media

An analysis of the experimental data suggests that the observed high acoustic absorption performance of the extruded products is largely attributed to their highly heterogeneous structure (Khan et al., (2005)) with a broad, complex pore size distribution. Four distinct approaches were chosen and compared. The first approach, here denoted by the Arbitrary Pore Size Distribution (APSD) method, is based on the numerical integration of the viscosity correction function through knowledge of the arbitrary probability density function for the pore size distribution (Horoshenkov et al. (2004)).

The second approach, denoted as the Double Porosity (DP) model, is based on the fact that, for many developed samples, the observed pore size distributions can be distinctively split into two scales, one around 10^{-4} m (the so-called “microscale”) and the other around 10^{-3} m (the so-called “mesoscale”), suggesting that wave propagation could be analogous to that observed in a double porosity medium (Only and Boutin,

(2003)) see Figure 4.3. The third approach based on the Pade approximation model is developed entirely on a set of four measurable non-acoustic parameters, which are the porosity, flow resistivity, tortuosity and the standard deviation of the log-normal distribution in the pore size. It is able to provide a very close fit (2-3%) to the measured data for loose and consolidated granular media (Horoshenkov et al. (1998)). The fourth approach was that proposed by Johnson-Allard (1997), which relies upon knowledge of the viscous and thermal characteristic lengths. The predictions by the models were validated against the experimental data measured using the standard method of standing wave apparatus (Song and Bolton (2000)).

4.3 Arbitrary Pore Size Distribution approach

The viscosity correction function, originally introduced by Biot (1956), is the ratio of the average viscous friction force on the capillary walls per unit bulk volume to the average seepage velocity per unit bulk cross-sectional area and measures the deviation from the Poiseuille flow friction. For a porous material modelled as a stack of circular cylindrical pores of radius (s) with an arbitrary probability density function $e(s)$, the viscosity correction function F is given by the following expression,

$$F(\omega) = \frac{1}{4} \frac{\int_0^{\infty} \sqrt{-i\lambda} T(\sqrt{-i\lambda}) e(s) ds}{\int_0^{\infty} \left[1 - \frac{2}{\sqrt{-i\lambda}} T(\sqrt{-i\lambda}) \right] e(s) ds}, \quad T(z) = \frac{J_1(z)}{J_0(z)}, \quad \lambda = s\sqrt{\omega\rho_0/\eta} \quad (4.1)$$

where, J_1 and J_0 are the modified Bessel functions (of the first kind) of the first and zero order respectively, ρ_0 the static fluid density and η the dynamic viscosity of air. The estimation of the viscosity correction function through a direct numerical

integration approach only requires data on the probability density function of the pore size distribution. The complex dynamic density ρ_b and complex dynamic compressibility C_b are then computed by the following relations, provided that the porosity (ϕ), flow resistivity (σ) and tortuosity (α_∞), of the material are known:

$$\rho_b(\omega) = \frac{\alpha_\infty}{\phi} \left(\rho_0 - \frac{\phi\sigma}{j\omega\alpha_\infty} F(\omega) \right) \quad (4.2)$$

$$C_b(\omega) = \frac{\phi}{\gamma P_0} \left(\gamma - \frac{\gamma - 1}{1 - \frac{\Omega\sigma}{j\omega\alpha_\infty\rho_0\text{Pr}} F(\omega\text{Pr})} \right) \quad (4.3)$$

where, γ is the specific heat ratio, P_0 is the ambient pressure and Pr is the Prandtl number. Finally, the dynamic density and the complex compressibility can be used to compute the normalised characteristic impedance (z_c), the complex wave number (k_c) and the normalised surface impedance (z_s) for a hard-backed sample of thickness (d),

$$z_c = \frac{1}{\rho_0 c} \sqrt{\frac{\rho_b}{C_b}} \quad (4.4)$$

$$k_c = \omega \sqrt{\rho_b C_b} \quad (4.5)$$

$$z_s = z_c \coth(-jk_c d) \quad (4.6)$$

where, c is the sound speed in air.

4.4 Double Porosity approach

The general double porosity theory developed by Olny and Boutin (2003), can be employed to model the acoustic behaviour of materials with two distinct pore scales: meso-porous scale, l_p , and micro-porous scale, l_m .

Three samples manufactured with different water to binder ratios, were tested. Their non-acoustical macroscopic parameters, the flow resistivity, porosity and tortuosity are summarized in Table 4.1.

Table 4.1: Shows non-acoustic properties of three extruded samples

Sample	ES01	ES02	ES03
Flow resistivity	6500	4000	1300
Open porosity	0.81	0.81	0.80
Tortuosity	1.58	1.73	1.26

From a close examination of the optical analysis probability density function (PDF) data (Khan et al., (2005) for the pore size distribution in materials ES02 and ES03 (Figure 4.26), it can be argued that the ratio between the characteristic dimensions of the meso- and micro-porous parts should be $l_p / l_m \approx 10$. The subscripts p , m , db have been adopted to denote the quantities related to mesopores, micropores and to the multiscale medium, respectively. According to the expressions presented in the work by Olny and Boutin (2003) the porosities can be computed by the aforementioned optical-counting technique according to which the overall areas attributed to the micro- and the meso-pores can be discriminated. Assuming that the areas occupied by micro- and

meso-pores, A_{fm} and A_{fp} , respectively, and employing Eq. (14) in reference of Only and Boutin (2003) we obtain

$$\phi_{db} = \phi_p + \phi_m (1 - \phi_p) = \frac{A_{fp}}{A} + \left(1 - \frac{A_{fp}}{A}\right) \frac{A_{fm}}{(A - A_{fp})} \quad (4.7)$$

where, A is the total area of the sample surface.

Regarding the flow resistivity (σ), the micro- and meso-pores can simply be considered as tubes acting in parallel.

$$\frac{1}{\sigma_{db}} = \left[\frac{(1 - \phi_p)}{\sigma_m} + \frac{1}{\sigma_p} \right] \quad (4.8)$$

Therefore, according to Eq. (84) in reference of Only and Boutin (2003) a rough estimation of the flow resistivity to be attributed to the micro-porous media could be obtained from the following,

$$\sigma_m = \frac{8\eta q_m^2}{\langle s_m \rangle^2 \Omega_m}, \quad \langle s_m \rangle \cong \int_{s_{\min}}^{s_{\max}} s_m \cdot e(s_m) ds \quad (4.9)$$

being η the air dynamic viscosity and $\langle s_m \rangle$ the mean micro-pore size calculated from the PDF of the micro-pores within the effective pore size range, $[s_{\min}, s_{\max}]$.

As a first approximation, the tortuosity can be considered equal at meso- and micro-pore scales. Such an assumption is justified assuming that both the micro- and meso-pores are the consequence of the same process of gas release, bubble formation and collapse.

The semi-phenomenological models of Johnson et al. (1987) and Lafarge et al. (1997) were adopted to estimate the viscous and thermal dynamic permeabilities, Π and Θ , respectively. i.e.

$$\Pi_i(\omega) = \Pi_i(0) \left(\left(1 - j \frac{M_i}{2} \frac{\omega}{\omega_{v,i}} \right)^{1/2} - j \frac{\omega}{\omega_{v,i}} \right)^{-1}, \quad \omega_{v,i} = \frac{\eta \Omega_i}{\rho_0 q_i^2 \Pi_i(0)} \quad (i = m, p) \quad (4.10)$$

$$\Theta_i(\omega) = \Theta_i(0) \left(\left(1 - j \frac{M'_i}{2} \frac{\omega}{\omega_{t,i}} \right)^{1/2} - j \frac{\omega}{\omega_{t,i}} \right)^{-1}, \quad \Theta_i(0) = \frac{\kappa q_i^2 \Pi_i(0)}{C_p \eta} \quad (i = m, p) \quad (4.11)$$

where κ is the thermal conductivity and C_p is the specific heat of air at constant pressure. In a first approximation, it was assumed that the thermal characteristic frequencies $\omega_{t,i}$ matched their viscous counterparts $\omega_{v,i}$. and that the dimensionless shape factors M and M' were equal to 1 to avoid the ambiguity in defining the thermal static permeability constant. The complex dynamic density (ρ_{db}), and complex dynamic compressibility (C_{db}), of the double porosity medium were then computed through the expression suggested by Olny and Boutin (see Eq. (85) and (80) in reference of Olny and Boutin (2003)).

$$\rho_{db}(\omega) = j \frac{\eta}{\omega} \left((1 - \Omega_p) \Pi_m(\omega) + \Pi_p(\omega) \right)^{-1} \quad (4.12)$$

$$K_i(\omega) = \frac{\gamma P_0}{\Omega_i} \left(\gamma + j(\gamma - 1) \frac{\Theta_i(\omega)}{\delta_i^2 \Omega_i} \right)^{-1}, \quad \delta_i^2 = \frac{\kappa}{\rho_0 C_p \omega} \quad (i = m, p) \quad (4.13)$$

$$C_{db}(\omega) = \left(\frac{(1 - \Omega_p)}{K_m(\omega)} + \frac{1}{K_p(\omega)} \right) \quad (4.14)$$

where δ_i is the thermal skin depth. Characteristic and surface impedances, together with the complex wavenumber, were then calculated through Eq. (4.4)-(4.6).

4.5 Pade Approximation

The prediction of the acoustic properties of many porous materials relies heavily on accurate information about the pore size distribution. Here we are referring to highly heterogeneous porous media which are characterised by a range of very different pore sizes. These materials have many different origins. For example, in geophysics they come in the form of porous stones with pronounced cracks, in the food industry they come in the form of breads and cornflakes, in the automotive industry as ceramic catalytic converters for vehicle exhausts.

If a porous medium is composed of pores of two very distinct sizes (e.g. a layer of fibreglass with artificially drilled holes), then the dual-porosity models discussed in the previous section can be adopted. In many types of porous media, including recycled porous media, a discrete separation of pore scales is not obvious and the application of the dual-porosity model is problematic partly due to the required large number of the input material parameters (Boutin et al. (1998)). In a particular case of materials with pore size distribution close to log-normal the viscosity correction function can be given by a very simple polynomial ratio (Horoshenkov et al., (1998)).

$$F(\varepsilon) \cong \frac{1 + a_1\varepsilon + a_2\varepsilon^2}{1 + b_1\varepsilon} \quad (4.15)$$

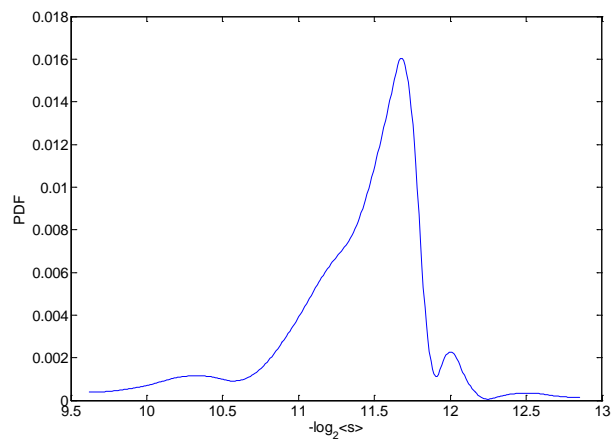
in which a_1, a_2 and b_1 are real coefficients with values that only depend on the pore geometry. The frequency dependant parameter,

$$\varepsilon = \left(\frac{-i\omega\alpha_\infty\rho_0}{\sigma\Omega} \right)^{1/2}$$

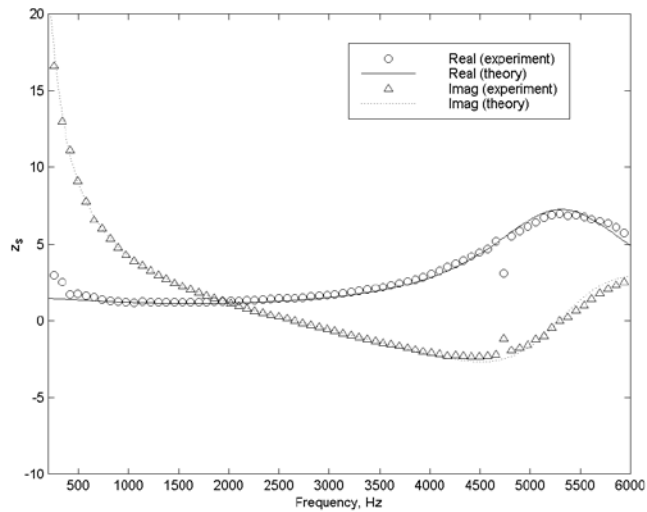
is an equivalent to the ratio of the mean pore radius to the viscous boundary layer thickness. The frequency dependent parameter is equivalent to the ratio of the mean pore radius to the viscous boundary layer thickness. In a particular case, then the pore can be assumed to be of circular cross-section, the coefficients are $a_1 = b_1 = \theta_1 / \theta_2$ and $a_2 = \theta_1$ where $\theta_1 = 4/3e^{4c} - 1$, $\theta_2 = \sqrt{1/2}e^{3/2c}$, $c = (\delta\mu \log(2))^2$ and $\delta\mu$ is the standard deviation in the log-normal pore size distribution. An example of the application of this model to predict the normalised surface acoustic impedance of a 20mm hard-backed layer of coustone is shown in Figure 4.2. Coustone material (see Figure 4.2(a)) is a type of consolidated flint aggregate which is inherently porous. This material is normally used for noise control in hostile environments which require absorbers with a good structural strength. The macroscopic properties and pore size distribution of this material have been measured using the laboratory facilities available in the University of Bradford which are discussed in sections 4.7 to 4.16. The PDF data on the pore size distribution is shown in Figure 4.2(b). The values of the macroscopic parameters for this material are: $\sigma = 31.5 \text{ kPa s m}^{-2}$, $\phi = 0.40$, $\alpha_\infty = 1.66$, and $h = 0.021 \text{ m}$. Figure 4.2(c) presents the measured and predicted data for the real and imaginary parts of the normalised surface impedance of the 20mm hard-backed layer of coustone. The estimated error in the prediction is within 2%.



(a)



(b)



(c)

Figure 4.2: Microscopic photograph of the Coustone structure (a), the probability density function for its pore size distribution (b) and the normalised surface impedance of a 20 mm hard-backed layer of Coustone (c).

However, in many porous materials the pore size distribution is far from log-normal. As an example, Figure 4.3(a) shows the complex pore size distribution data ($e(s)$) obtained from magnified optical images of a typical extruded material. The data shows that the pore size distribution cannot be approximated with a log-normal fit. In order to overcome this deficiency, it is possible to use direct numerical integration of the expressions for the average seepage velocity (denominator) and the frictional force (numerator) in the viscosity correction function as suggested by Eq. (4.1) (Horoshenkov et al. (2004)), i.e. expressions (4.1)-(4.3) were used together with the pore size distribution data (Figure 4.2(b)) to calculate the normalised surface impedance of a 30mm hard-backed layer, the extruded porous material (ES03) depicted in Figure 4.3(b). The other non-acoustic parameters were measured using the laboratory facilities at the University of Bradford. These parameters were: $\sigma = 1950 \text{ Pa s m}^{-2}$, $\phi = 0.80$, $\alpha_{\infty} = 1.56$, $h = 0.030 \text{ m}$. There is an excellent agreement (3% error) between the measured and predicted data. Similar results were obtained when this approach was used to predict the impedance of a porous acoustic underlay. It was demonstrated that the pore size distribution of such a material is significantly inhomogeneous so that a log-normal fit could not be assumed. An attempt to use the best log-normal fit resulted in a very large (>100%) error in the real part of the surface impedance.

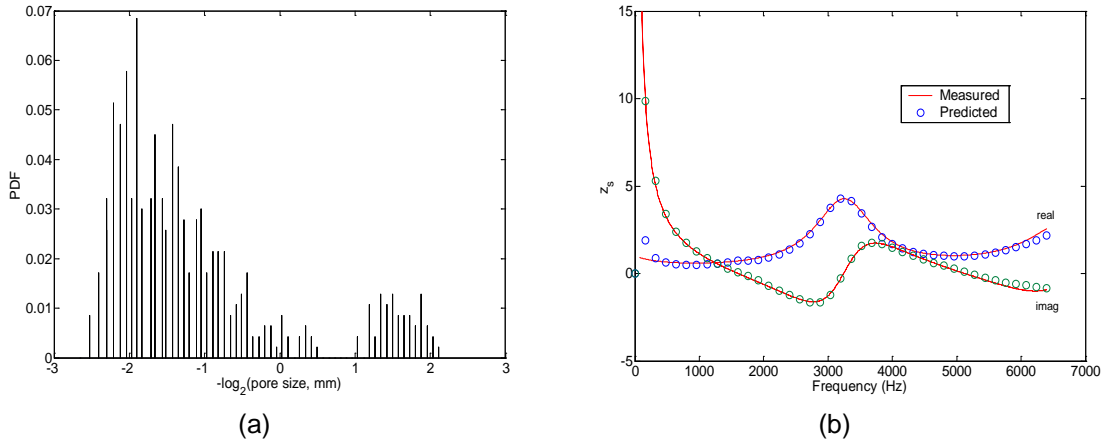


Figure 4.3: The pore size distribution (a) and the acoustic surface impedance (b) of a 30mm hard-backed layer of extruded recycled material.

4.6 Johnson-Champoux Allard Model

Champoux and Allard (1987) based on the previous work by Johnson et al (1991) introduced an expression for the dynamic bulk modulus for a broad range of porous materials. The characteristic lengths Λ and Λ' were used to describe the high frequency behaviour of the dynamic density $\rho_b(\omega)$ and of the bulk modulus $K_b(\omega)$ of air in porous materials so that the characteristic impedance and complex wavenumber in a porous medium could be predicted.

Two parameters are involved in the calculation of the dynamic bulk modulus, the open porosity ϕ , and the thermal characteristic length Λ' .

$$\check{K}(\omega) = \frac{\gamma P_0 / \phi}{\gamma - (\gamma - 1) \left[1 - j \frac{8k}{\Lambda'^2 C_p \rho_0 \omega} \sqrt{1 + j \frac{\Lambda'^2 C_p \rho_0 \omega}{16k}} \right]^{-1}} \quad (4.16)$$

where, γ is the specific heat ratio of air and P_0 is the air equilibrium pressure.

4.7 Characterisation methods for acoustic materials

The models presented in sections 4.3 to 4.6 rely upon the knowledge of several non-acoustical parameters which relate to the micro-structure of the porous medium. The key non-acoustical macroscopic parameters are the flow resistivity, porosity and tortuosity. These can be estimated with standard testing methods which are summarised in the following sections.

The physical testing of the materials can be classified into two main groups:

- i. Acoustic
 - Large and small impedance tube
 - Impact sound insulation
- ii. Non-acoustic
 - Open porosity
 - Air flow resistivity
 - Dynamic stiffness
 - Tortuosity
 - Thermal conductivity
 - Rate of reaction

4.8 Large and small impedance tube

There are many different methods that can be used to determine the acoustic properties of materials. The techniques mainly involve exposing the material to known sound fields and measuring the effect of the materials presence on the sound field. The acoustic characteristics of materials are determined in terms of absorption, reflection,

impedance, admittance, and transmission loss (Song and Bolton, (2000)). The acoustic properties that can be determined from an impedance tube experiment are:

- i. Reflection coefficient
- ii. Normal incidence absorption coefficient
- iii. Impedance ratio
- iv. Admittance ratio

The most useful engineering property in the above list is the normal incidence absorption coefficient which is a function of frequency valued between zero and one. Sound absorption is the proportion of sound energy being absorbed by the material. This is the primary engineering indicator to how well an acoustic material can remove sound energy from a given environment. The standard BS EN ISO 10534-2 (20010 (see also ASTM E 1050 (2008)) describes the method that has come to be known as the “two microphone” or the “transfer function method” of measuring absorption and impedance of acoustic materials. The standard establishes acceptable conditions under which reliable data on the acoustical performance of a material specimen can be obtained. Standard impedance tube equipment is shown in Figure 4.4. The two microphone method is shown schematically in Figure 4.5.

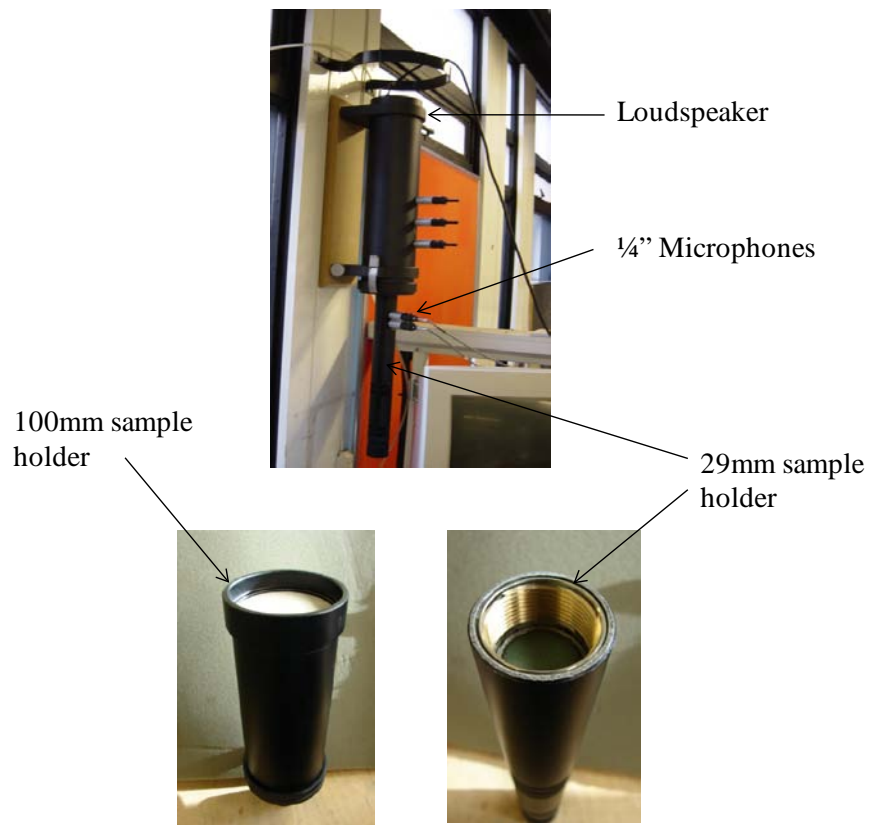


Figure 4.4: The two microphone impedance tube

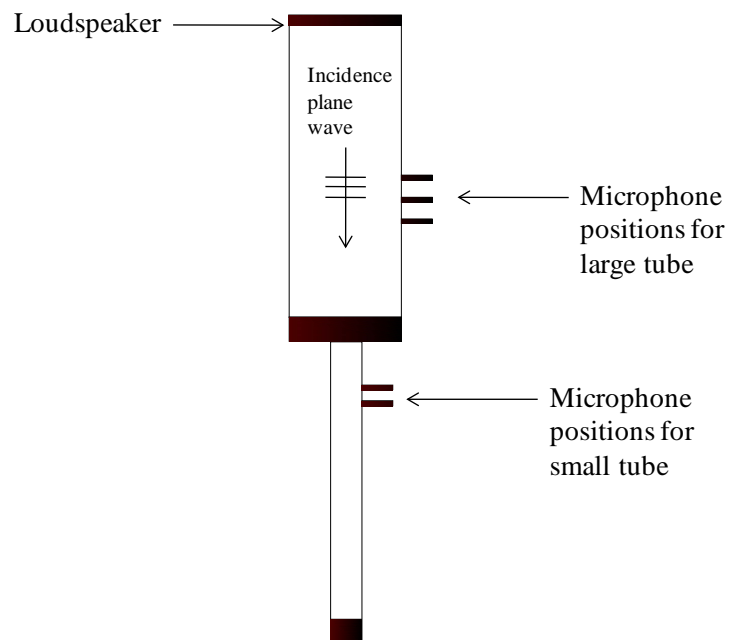


Figure 4.5: Schematic of the two microphone impedance tube

The measurements were carried out using a large and small Bruel and Kjar type 4206 impedance tube. The required size of the tested sample was 29mm diameter for the small impedance tube and 100mm diameter for the large impedance tube measurement and the sample thickness was 30mm \pm 1mm.

The sample of the material to be tested was placed in the sample holder. A rigid plunger with an adjustable depth was placed behind the sample to provide a reflecting surface. A sound source (loudspeaker) was at the opposite end of the tube. The adjustable electronic filter was provided and it had three settings, low pass, high pass, and linear. The low pass filter was used to collect high resolution acoustic data in the frequency range of 50-1600 Hz. The high pass filter was used for data collection in the small tube in the frequency range of 500 – 6400 Hz.

Pair of ¼" Bruel & Kjar type 2670 microphones were mounted flush with the inner wall of the tube. The sound waves generated by the loudspeaker propagate into the impedance tube, some of the sound energy is reflected by the sample surface, creating an interference pattern inside the tube which is recorded and then related to the proportion of the sound energy reflected by the samples surface. The impedance tube speaker is driven by a Bruel and Kjar power amplifier, type 2703. The gap between the edge of the sample and the wall of the tube was avoided or sealed with sealing putty. Bruel and Kjar Pulse type 3560c analyser was used to control the impedance tube and analyse the data on the acoustic pressures measured on the two microphones. The impedance tube was mounted vertically in order to measure acoustic properties of loose granular material.

To understand the phenomena occurring inside the impedance tube a very basic type of sound signal needs to be studied. The acoustic pressure, p as a function of time and position is,

$$p = p_0 \cos(kx - \omega t + \phi_0) \quad (4.17)$$

where, p_0 is the amplitude, and ϕ_0 is the initial phase, k is the wavenumber, and ω is the angular frequency of the wave. Figure 4.6 shows a plane harmonic wave travelling in the x direction in a lossless medium.

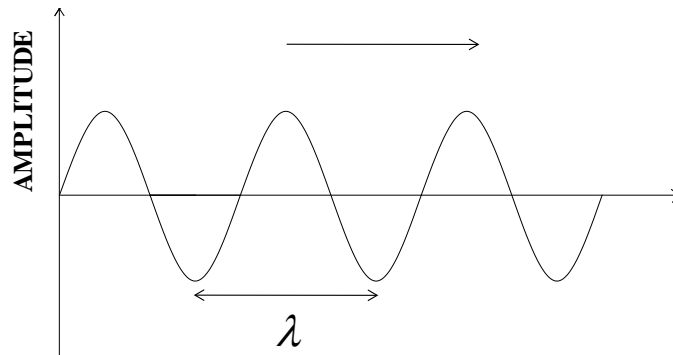


Figure 4.6: A plane harmonic wave

The total phase ϕ at position x and time t is,

$$\phi = kx - \omega t + \phi_0 \quad (4.18)$$

and the wave is plane because the wave fronts (surface of constant phase) are planes perpendicular to the x axis. The wavenumber, k , and the angular frequency, ω , are related respectively to the wavelength, λ , and frequency, f , of the wave as follows,

$$k = \frac{2\pi}{\lambda} \quad , \quad \omega = 2\pi f \quad (4.19)$$

The harmonic wave can be represented by the complex exponential,

$$p = p_0 e^{i(kx - \omega t + \phi_0)} \quad (4.20)$$

where, the physical wave (equation 4.18) is the real part of the complex quantity representing the sound wave.

In a lossless medium sound waves propagate with a constant speed, characteristic of the medium. For a harmonic wave the speed of sound is simply related to the wavelength and the frequency as follows,

$$c = \lambda f = \omega/k \quad (4.21)$$

If the medium is lossy, then the plane harmonic sound wave decays exponentially with distance,

$$p = p_0 e^{-\alpha x} \cdot e^{i(k' x - \omega t)} \quad (4.22)$$

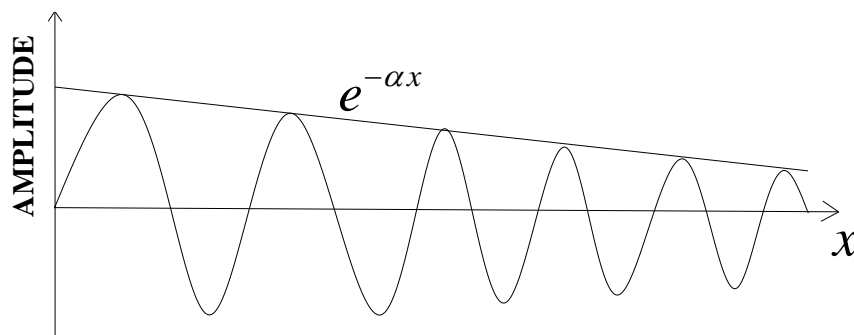


Figure 4.7: A wave decaying exponentially with distance

Figure 4.7, shows the behaviour of a harmonic wave in a lossy material, where p is the acoustic pressure at distance x from the reference point where the pressure is p_0 , and $k' = 2\pi/\lambda$ is the real part of the wavenumber, where λ is the wavelength, and (α) is

the attenuation coefficient. From equation 4.22 it follows that sound attenuation can be formally included in the wavenumber by defining a complex wavenumber,

$$k^* = k' + ik'' = k' + i \alpha \quad (4.23)$$

The expression for the sound wave now has the same form, $p = p_0 \exp[i(k^*x - \omega t)]$, as in a lossless medium. The complex wavenumber, substituted in equation 4.21, defines a complex sound speed for the material as follows,

$$c^* = \frac{\omega}{k^*} \quad (4.24)$$

However, the propagation of the wave as a function of space and time is still determined by the phase velocity, c which is related to the real part of the wavenumber,

$$c = \frac{\omega}{k'} \quad (4.25)$$

The function of the two microphones attached to the impedance tube is to take pressure readings [2], the sound pressure of the incident wave P_I and the reflected P_R are:

$$P_I = \hat{P}_I e^{jk_0x} \quad (4.26)$$

and

$$P_R = \hat{P}_R e^{-jk_0x} \quad (4.27)$$

where \hat{P}_I and \hat{P}_R are the magnitudes of P_I and P_R at the reference plane ($x = 0$) and k_0 is the wavenumber in air.

The sound pressures P_1 and P_2 on the two microphones are:

$$P_1 = \hat{P}_I e^{jk_0x_1} + \hat{P}_R e^{-jk_0x_1} \quad (4.28)$$

$$P_2 = \hat{P}_1 e^{jk_0 x_2} + \hat{P}_R e^{-jk_0 x_2} \quad (4.29)$$

The transfer function for the incident wave taken between the two microphones is:

$$H_I = \frac{P_{2I}}{P_{1I}} = e^{-jk_0(x_1-x_2)} = e^{-jk_0 s} \quad (4.30)$$

where, $s = x_1 - x_2$ is the microphone separation. Similarly the transfer function for the reflected wave is:

$$H_R = \frac{P_{2R}}{P_{1R}} = e^{jk_0(x_1-x_2)} = e^{jk_0 s} \quad (4.31)$$

The transfer function H_{12} for the total sound field may be obtained by using equations 4.28 and 4.29:

$$H_{12} = \frac{P_2}{P_1} = \frac{e^{jk_0 x_2} + r e^{-jk_0 x_2}}{e^{jk_0 x_1} + r e^{-jk_0 x_1}} \quad (4.32)$$

where r is the acoustic reflection coefficient, $r = P_R/P_I$.

Transposing equation (4.32) to yield r , and using equations (4.30) and (4.31), one has,

$$r = \frac{H_{12} - H_I}{H_R - H_{12}} e^{2jk_0 x_1} \quad (4.33)$$

From the reflection coefficient, the absorption coefficient α and normalised impedance $z/\rho_0 c$ of the sample may be determined from the following equations:

$$\alpha = 1 - |r|^2$$

and

$$z = \frac{Z}{\rho_0 c} = \frac{1+r}{1-r}$$

The British Standard (BS EN 1793-3) and ASTM E1050-08 specify a test method for assessing the sound absorption performance of noise reducing devices designed for roads. This standard gives a normalised traffic noise spectrum for the evaluation and assessment of the acoustic performance of devices designed to reduce traffic noise near roads.

Table 4.2: Normalised traffic noise spectrum

Frequency (Hz)	L_i (dB)
100	-20
125	-20
160	-18
200	-16
250	-15
315	-14
400	-13
500	-12
630	-11
800	-9
1000	-8
1250	-9
1600	-10
2000	-11
2500	-13
3150	-15
4000	-16
5000	-18

The spectrum (Table 4.2) that is used for the calculation of the acoustic performance of traffic noise reducing devices expressed in terms of a single number rating of sound absorption and airborne sound insulation for sound absorbing materials. A single number rating is derived to indicate the mean (weighted) performance of the product so

that various material formulations can be easily compared. The individual sound absorption coefficient is weighted according to the normalised traffic noise spectrum presented in Table 4.2. The single number rating of sound absorption DL_a , in decibels, is given by:

$$DL_a = -10 \log_{10} \left| 1 - \frac{\sum_{i=1}^{18} S_i^a 10^{0.1L_i}}{\sum_{i=1}^{18} 10^{0.1L_i}} \right| \quad (4.34)$$

4.9 Impact Sound Insulation test

A very useful property of porous elastic materials is their ability to insulate against impact sound. Most of the work for impact sound insulation is concerned with building acoustics problems. The testing of underlay samples designed for use in acoustic flooring systems must comply with Building Regulations Approved Document E and ISO 140 part 8. Rushforth et al. (2004) have studied acoustic and mechanical properties of underlay manufactured from recycled carpet waste. They manufactured small material specimens using a batch process and designed a small impact test rig which allowed for these specimens to be tested efficiently in the laboratory (see Figure 4.8). Davern (1988) carried out measurements of impact sound insulation on two timber floors with vinyl floor coverings on resilient layers. Owaki et al (1998) studied prediction of the floor impact sound insulation in multiple dwelling buildings, in which they measured the effect of various wooden floor coverings in actual buildings. Johansson (1995) focused on low frequency impact sound insulation of a light weight wooden joist floor, where he studied the effect of increasing the rigidity of joists and boards.

In this work the performance of the materials made from polymeric waste was investigated using a test rig after Rushforth et al. (2004) (see Figure 4.8). The impact

sound was measured in the form of the vibration which was caused by dropping a mass on the sample as illustrated in Figure 4.9.



Figure 4.8: Picture of the impact transmission rig

The underlay samples made using the polymeric waste were fixed to a 400mm long, 144mm wide and 18.2mm thick timber plank, which was designed to simulate a flooring system with a typical span between the joists. The floor section was clamped at either end to form a 200mm span of freely suspended 'floor'. The samples were then subjected to impacts from a brass cylinder dropped in a tube. An accelerometer attached to the underside of the 'floor system' was used to measure the level of vibration transmitted through the structure. A constant force of impact was applied sequentially to eight positions distributed over the top of the 140mm x 190 mm sample by dropping a 500g mass from a height of 40mm. The sample was firmly attached to the floorboard using double-sided adhesive layer. The height of the drop tube could be adjusted to

allow for different sample thicknesses whilst maintaining a constant drop height. Eight points of drop have been considered to determine the average impact insulation performance of the tested sample. The test was repeated in the absence of the sample to determine the relative impact sound insulation. Impact events were recorded digitally using WinMLS software.

An indication of the acoustic performance of the underlay was obtained by comparing the octave band acceleration spectra between 100 and 4000 Hz. The lower the amplitude of the transmitted vibration acceleration, the better performing was the sample under test. Accordingly, the acoustic performance of the carpet underlay was determined.

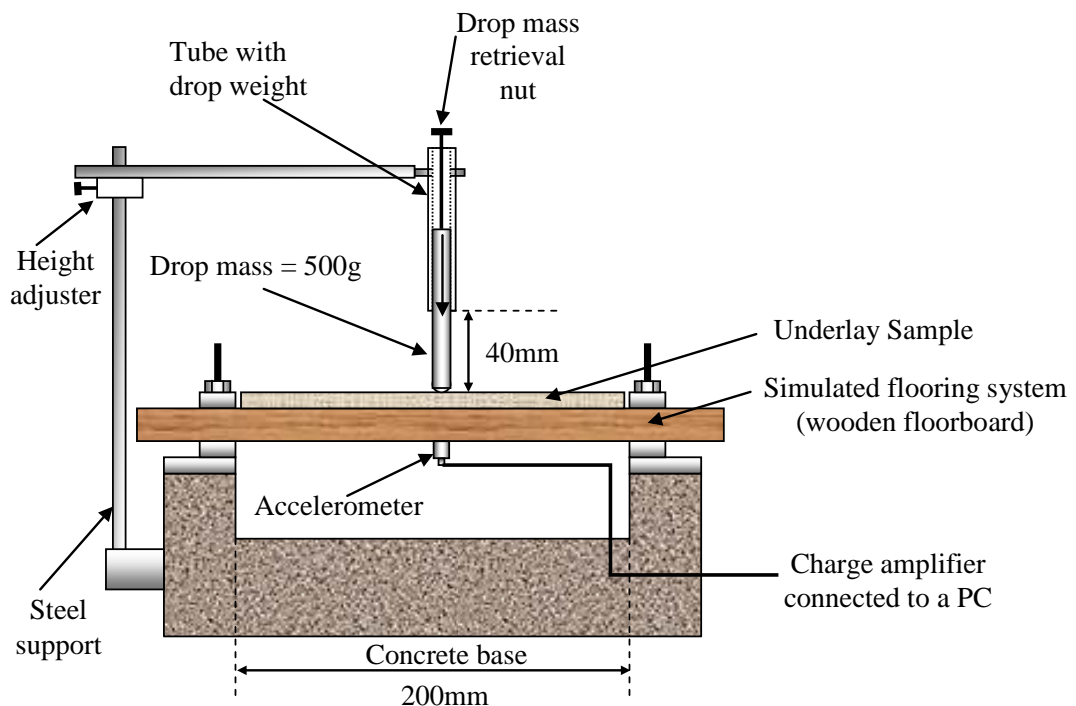


Figure 4.9: Schematic diagram of the impact transmission rig

The results of the tests were presented in the form of mean acceleration levels determined by averaging eight consecutive measurements using the following expression,

$$L_{AV} = 10 \log_{10} (1/M \sum_{i=1}^M 10^{L_{A_1 i}/10}) \quad (4.35)$$

where $M = 8$ is the number of measurements, and $L_{A_1 i}$ is the acceleration level for the i -th measurement (dB). The broadband acceleration level was predicted by,

$$L_{AV, BB} = 10 \log_{10} (\sum_{n=1}^N 10^{L_{AV}^{(n)}/10}) \quad (4.36)$$

where L_{AV}^n are the octave band levels and $N = 7$ is the number of octave band levels used in the analysis.

The result for the weight dropped directly on the wooden floor was also presented for comparative analysis. The impact sound transmission loss provided by the underlay sample can be determined from the following equation,

$$TL = L_{AV, wood} - L_{AV, sample} \quad (4.37)$$

where the acceleration level due to the weight is $L_{AV, wood}$ dropped directly on the bare wooden floor and $L_{AV, sample}$ is the acceleration level due to the weight dropped on the floor covered with underlay.

4.10 Measurement of some related non-acoustical material properties

The experimental methods used to measure the non-acoustic properties of porous materials are presented in this section.

4.11 Porosity measurement

Section 4.3 to 4.6 presented several models for the acoustical properties of porous media. All of these models require the knowledge of porosity. Various methods are available for measuring porosity such as mercury porosimetry, buoyancy, or methods based on density measurements can be found in the work done by Bourbie on acoustics of porous media (1987). The porosity of a porous material corresponds to the volume proportion of fluid contained in the pores, i.e. the total volume of the fluid in the pores divided by the volume of the sample. Porosities can be defined as open, trapped, or total porosity depending on the methods selected. Porosity is an essential parameter in the physical and acoustical modelling of porous media.

There are no agreed standard procedures for measuring the proportion of open, interconnected pores (open porosity) which is required for acoustic modelling. Intuitively, one can assume that the open porosity is equal to the true porosity which can be determined from the data on the density of the material frame (ρ_f) and the density of the material itself (ρ_m). In this case the true porosity value should simply be $\Omega \cong 1 - \rho_m / \rho_f$. In reality, the true porosity value may not necessarily be equal to the proportion of open, interconnected pores which determines the actual ability of sound energy to penetrate the porous medium. One direct method for measuring the open porosity is to make use of the Boyles's law ($pV = \text{const}, T = \text{const}$). Another common method involves the saturation of the sample with water. The density of the dry sample and the density of the sample when saturated with water provide an evaluation of the porosity. The latter method is not always appropriate as it can damage the sample or modify its morphological properties.

In the former method, a porous sample is introduced in an air tight chamber that is connected to a U-tube monometer. Based on this principle, Champoux et al. (1991) designed a much more intricate system providing results with excellent precision in a wide range of porosities. Their system involves a micrometer drive for precise variations of volume in the chamber, a sensitive differential pressure transducer to replace the U-tube manometer, and a large air reservoir to isolate the apparatus from atmospheric pressure fluctuation.

Recently, an improved method based on comparison of air volumes has been proposed by Leclaire (2003). Unlike the original method detailed by Beranek (1942), the proposed method automatically compensates for any temperature or pressure fluctuations which may affect the value of the pV product. The method described in this section is based on the compressibility of the air in the connected pores and therefore this method yields the open porosity. The equipment for measuring the porosity is shown in Figure 4.10. The experimental principle of the method itself is shown in Figure 4.11.

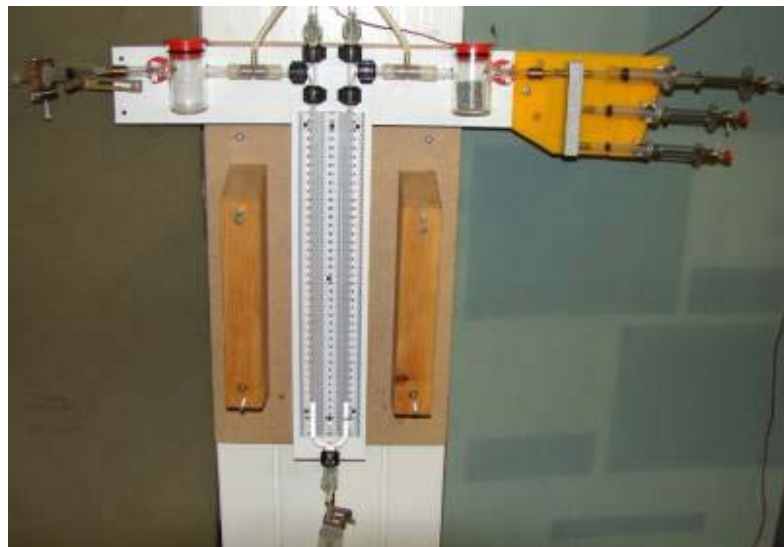


Figure 4.10: Experiment setup for the measurement of porosity

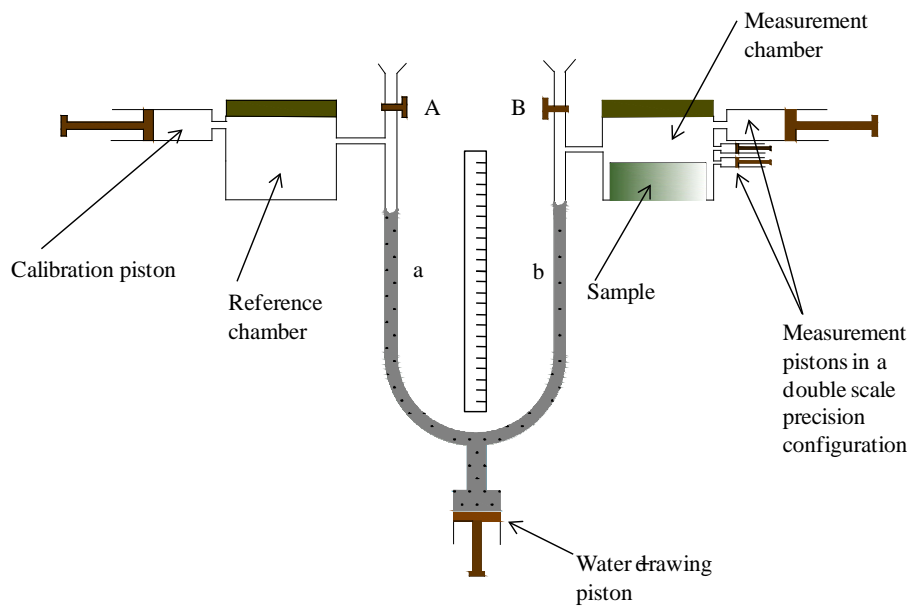


Figure 4.11: Schematic diagram of the air volume comparison system

The setup in the Acoustics Laboratory at the University of Bradford consists of two 60 ml reference and measurement chambers, a U-tube manometer, calibration, water drawing and air volume measurement pistons. Two air tight chambers are connected to the branches of a U-tube manometer containing water. The manometer is made up of glass tubes with an inner diameter around 5mm, large enough to neglect capillary effects. Water can be removed from and re-injected in the monometer with the help of a water drawing piston. If valves A and B are closed, drawing water will have the effect of increasing both the reference volume and the volume in which the sample is contained. A measurement piston of 20 ml capacity and two smaller pistons of 10 ml capacity are connected to the measurement chamber.

In order to equalise the volumes of the reference chamber and the measurement chamber in the absence of sample and with the measurement piston set to zero a calibration experiment is carried out initially. The two chambers are first set at atmospheric pressure (valve A and B opened) and starting from a high level of water in

both branches, A and B are closed and water is drawn. If the volumes of the two chambers are identical, the pressure difference ($a - b$) would be zero. Equalising the two volumes can be achieved by the calibration piston. The idea of the larger measurement piston is to provide a gross value of the volume while the smaller pistons can be used for fine tuning. The capacity of the smaller pistons should correspond to a convenient integer number of the unit graduation on the larger piston, for example, 1 ml capacity for 1 ml unit graduation.

After the calibration has been completed, a porous sample is placed in the measurement chamber. This is done after the two chambers are set at atmospheric pressure (A and B opened). The reduction in the volume of air due to the introduction of the porous solid is compensated by varying the volume of the measurement piston (starting from the zero position). The measurement piston should be moved only when B is open. After each movement of the water drawing piston, the chambers are returned to atmospheric pressure by opening A and B. As water is drawn in the successive tries (with A and B closed), the difference in head levels ($a - b$) between the two branches of the manometer approaches zero when the volume in the measurement piston corresponds to the volume of solid of the porous sample. The proportion of solid (i.e. porosity) is obtained by dividing the volume of solid by the volume of the sample.

4.12 Flow resistivity

Another important non-acoustic property needed to predict the acoustic absorption performance of porous media is their flow resistivity. Various methods are reported in literature for measuring flow resistivity of porous materials. These methods are based essentially on forcing a steady state or slowly oscillating air flow through a sample of

the porous material. The measurement of both the volume flow rate and the differential pressure across the sample yields the air flow resistance of the sample (Bies et al., (1980) and ISO9053:2 (1989). Suitable measurement procedures are reported in the international standard ISO 9053 (1991). A typical experimental set up for measuring the flow resistivity is shown in Figure 4.12.

The air flow resistivity is the air flow resistance per unit material thickness and it has the units of N.s/m^4 or Pa.s.m^{-2} . The ISO 9053 reports a standard method for the measurement of the air flow resistance. It is based on the measurement of the sound pressure in a small chamber having rigid walls. A slow air flow with the velocity of less than 5 mm/s is created through the specimen as shown in Figures 4.12 and 4.13. The value of the flow resistivity determines the ability of sound wave to penetrate the material and attenuate. The flow resistivities of useful noise control materials vary widely, but typically fall within the range 1000 to 100,000 N.s/m^4 . The flow resistivity is usually taken to be a measure of the viscous coupling between the fluid and solid phases of the porous material, and so is a measure of the potential for viscous dissipation of sound. At a microscopic level, flow resistance results from the formation of a viscous boundary layer as fluid (air) flows over each particular solid frame, and the amount of shearing in those boundary layers. Hence, the amount of viscous drag per unit mass of particles exerted by the flow on the frame medium, increases as the mean particle radius decreases.

In the setup shown in Figure 4.13 compressed air is directed towards the material sample through a smooth glass funnel. Differential pressure transducers are used to measure the pressure difference ΔP , air flow resistivity σ is given as:

$$\sigma = \frac{\Delta P \cdot S}{Ql} = \left[\frac{\text{N}_s}{\text{m}^4} \right] \quad (4.38)$$

where, Q is the flow rate in m^3/s , l is the sample thickness in m, S is the area of the circular sample in m^2 .

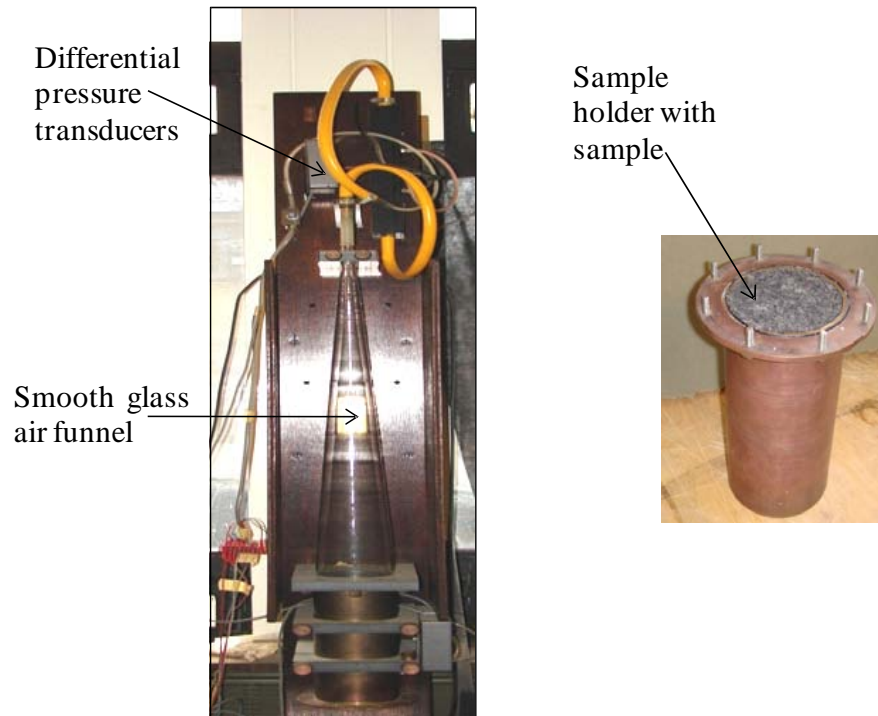


Figure 4.12: Setup of air flow resistivity apparatus

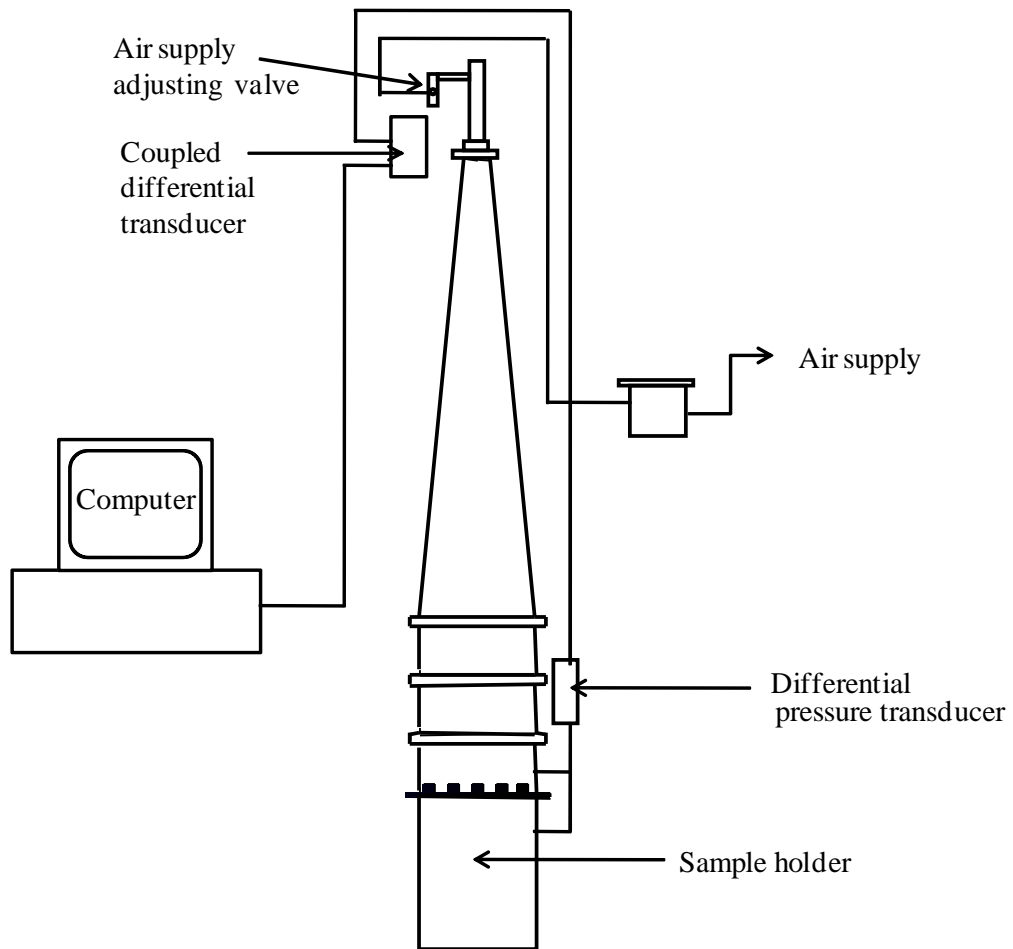


Figure 4.13: Schematic of flow resistivity apparatus

A circular sample of 100mm diameter was inserted into the sample holder. The sample was sealed around the circular edges with putty or tape in order to prevent air leakage. The air flow was controlled using a precision valve; the flow rate was measured in the range of 0.3-5 litre/min. The valve is increased slowly to change the air discharge in 0.3-0.5 litre/min steps in 30-40 seconds.

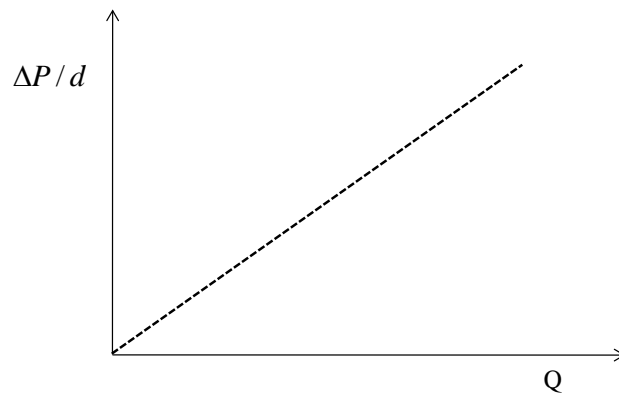


Figure 4.14: Pressure drop versus volume flow rate

The flow resistivity depends on the porosity of a material as well as its tortuosity, the steady state flow resistivity of porous materials is a nonlinear function of flow velocity owing to inertial effects and to turbulence at very high flow rates. Tests should be conducted at low flow rates to fall within the linear regime, since the linear flow resistivity is appropriate for acoustical situations in which particle velocities are typically on the order of several mm/s or less. The pressure difference across the test sample can be measured by using differential pressure transducers, and airflow velocities are usually inferred from the volume flow rate through the sample.

4.13 Dynamic stiffness

In order to reduce the transmission of structural vibrations, materials used in the building industry are mainly resilient materials such as foams or mineral wool. They can be a part of a floating floor, which consists of a slab lying on the resilient material, and the resilient material is usually termed insulation layer because they help to reduce the sound pressure level due to the impact. The performance of the floating floor directly depends on the mechanical properties of the insulation layer, together with its

mass per unit area. A simple way to predict the impact sound insulation performance of a porous elastic layer is to measure its dynamic stiffness. A measure of the dynamic stiffness allows the calculation of the dB reduction in the transmitted sound pressure level. This is because the transmission of sound as function of frequency reduces by approximately 30 dB per decade to the real resonance frequency of floating slab-resilient layer, as indicated in following relation $DL = 30 \log_{10}(\frac{f}{f_{res}})$, where f_{res} is the frequency of the mechanical resonance of the resilient flooring system. According to the standard method detailed in BS 29052-1 (1989), a material sample is loaded with greater than 0.4 kPa in the case of wall insulation material or equal to or less than 4 kPa in the case of machinery foundation materials. By testing small sample of resilient material proves to be particularly effective in terms of time since measuring the dynamic stiffness of the sample is fast, whereas performing a full scale measurement of the impact level requires a longer period of time.

The dynamic stiffness, S , of a resilient layer, in N/m^3 , can be expressed in terms of its Young's modulus E and initial thickness L_o ,

$$S = \frac{E}{L_o} \quad (4.39)$$

since

$$E = \frac{L_o}{\Delta L} \times \frac{F}{A} \quad (4.40)$$

where F is the dynamic force acting perpendicular to the sample, A is the area of the sample and ΔL the variation of length of the sample due to the force acting on it. The above equation becomes,

$$S = \frac{F/A}{\Delta L} \quad (4.41)$$

In terms of the resonant frequency, the apparent dynamic stiffness is expressed as,

$$S = m(2\pi f_{res})^2 \quad (4.42)$$

or, equivalently

$$f_{res} = \frac{1}{2\pi} \sqrt{\frac{S}{m}} \quad (4.43)$$

with m being the total mass/unit area placed on top of the material during the test including shaker, accelerometers etc. Figure 4.15 shows a picture of the experimental setup with circular resilient material.

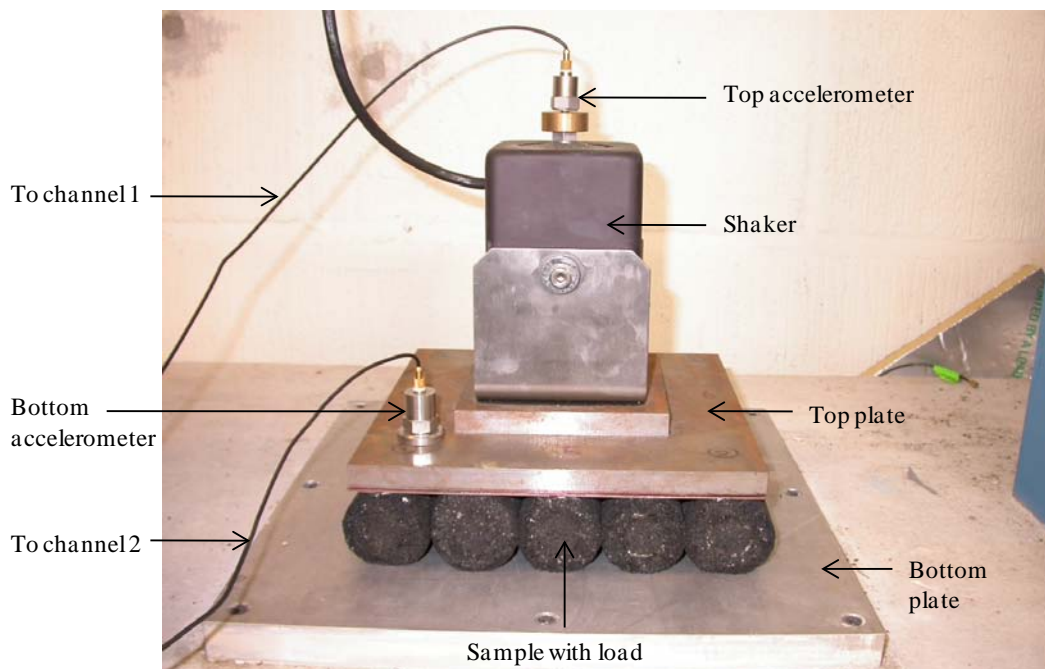


Figure 4.15: Showing setup of dynamic stiffness (BS29052) apparatus

The setup consists of charge amplifiers, two accelerometers one attached to the top plate and the other to the top of the shaker. The shaker is connected to the computer via a power amplifier. The loading plate is a steel plate of dimensions 20 x 20 cm². The weight of the top plate with the shaker and accelerometers is 8.05 kg. This plate is placed on top of the 20 x 20 cm² resilient material which must have a smooth surface. These recommended sample dimensions should be maintained within ± 2 mm. The shaker fixed to the top plate is excited using a sine sweep or white noise in a broad frequency band. The response is measured at eight different positions on the top plate. The excitations result in a resonance curve showing different peaks corresponding to each mode of vibration, the first resonance is required to calculate the dynamic stiffness (see Figure 4.16).

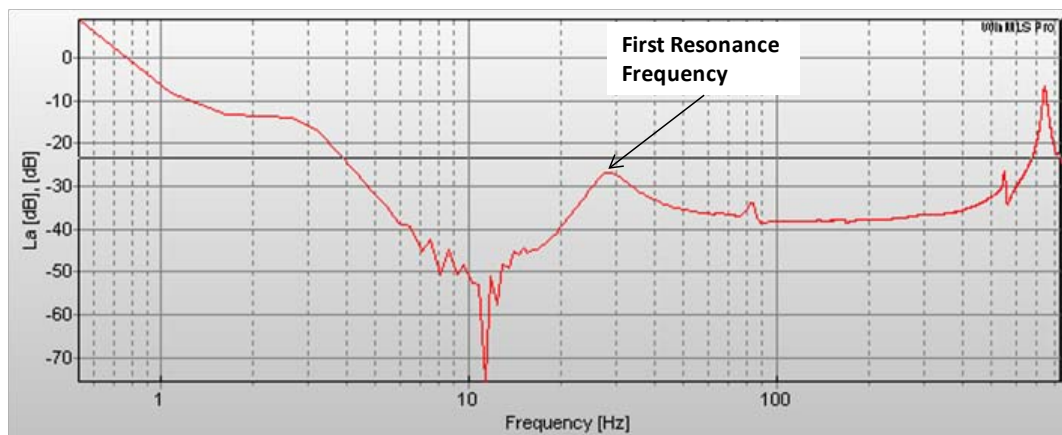


Figure 4.16: First resonance frequency

The software WinMLS was used to control the experiment and to calculate the acceleration spectra.

4.14 Tortuosity

An important non-acoustical property which determines the high-frequency acoustical behaviour of a porous layer is the tortuosity. Physically, the tortuosity accounts for the twistiness of the pores in a material. The first definitions of tortuosity came from Zwikker and Kosten in their classic book (1949) which discussed the so-called structure factor (k_s) (Figure 4.17). Further studies have been carried out by Attenborough (1983) and Johnson who provided a more precise definition for the tortuosity in a porous medium (1987).

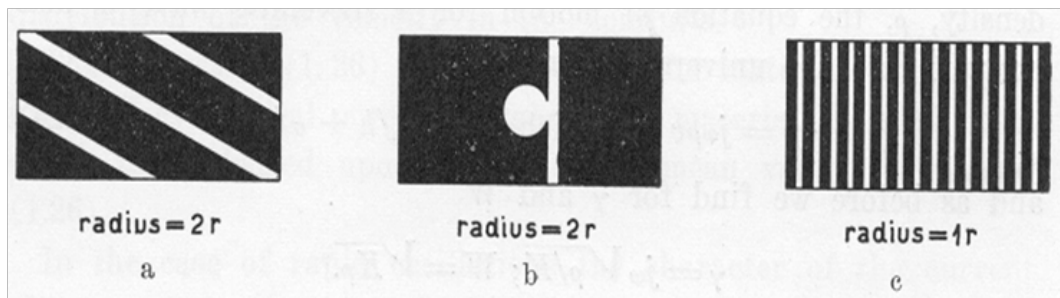


Figure 4.17: Diagrams on the definition of tortuosity (Zwikker and Kosten, (1949))

In its simplest case the twistiness of the pores relates to the ratio of the actual path (h_e) taken by a high frequency sound in the porous sample to the sample thickness,

$$\alpha_\infty \cong \frac{h_e}{h} \quad (4.44)$$

In porous media saturated by a viscous fluid the value of tortuosity is always $\alpha_\infty > 1$ even in the case when sound propagates in a straight pore at normal angle of incidence. The more common general definition of the tortuosity is given by Johnson and it is expressed as the ratio of two volume integrals,

$$\alpha_{\infty} = \int_{\Lambda} v^2 dV \left[\int_{\Lambda} v n dV \right]^{-2} \quad (4.45)$$

where v is the oscillatory flow velocity and n the unit vector in the direction of sound propagation. This ratio accounts for the deviation of the velocity vector from the straight path parallel to the wavenumber vector in the incident sound wave. It is particularly useful when the ratio $\alpha_{\infty} \cong h_e/h$ cannot be clearly defined and is complicated by several constrictions and expansions along the pore path (Figure 4.17.b).



Figure 4.18: Photograph of the tortuosity rig

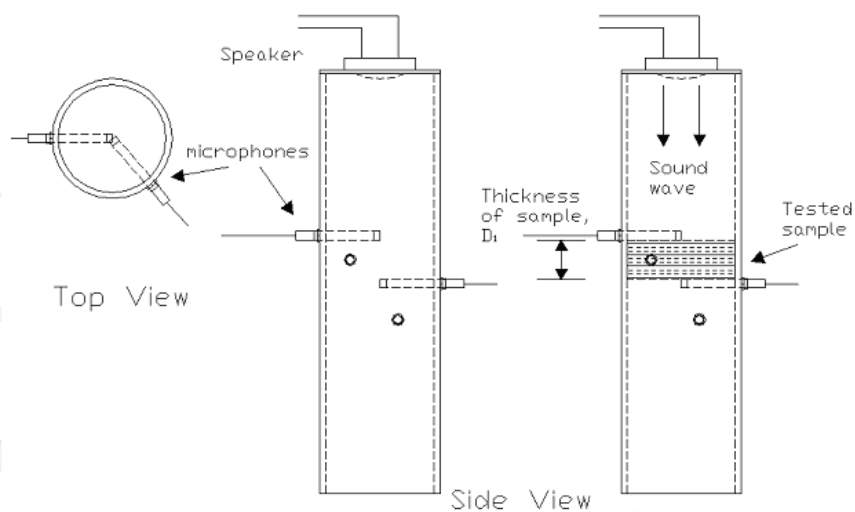


Figure 4.19: Schematic representation of the tortuosity rig

There are several methods of measuring tortuosity the majority of which are indirect. Here we detail three particular methods which were used in this work. The first method was proposed by Allard in 1994 and based on the ultrasonic time of flight in the porous medium (Allard, (1994)). The method assumes that at high frequencies the thickness of the viscous boundary layer is still considerably smaller than the characteristic pore dimension, i.e. $\lambda_V = s\sqrt{\omega\rho_0/\eta} \gg 1$. At these frequencies the phase velocity of the sound wave in the porous medium approaches $c_b \cong c_0/\sqrt{\alpha_\infty}$. For a typical noise control material with mean pore size of 100 μm (e.g. fibreglass) this regime is attained at $f > 25000 \text{ Hz}$ ($\lambda_V > 10$). A typical setup which has been developed at Bradford for measuring the tortuosity from the ultrasonic time of flight is shown in Figure 4.18. A high-frequency tweeter is mounted at the top of a PVC tube. A 48 kHz ultrasound wave is transmitted from the tweeter and received by the two 1/4'' microphones mounted on the top and on the bottom of the sample and their centres are aligned with the centres of both the sample and the tweeter as shown schematically in Figure 4.19. A separate measurement is carried out in the absence of the sample to determine the actual sound speed in air. The phase speed in the sample is measured by comparing the time delay (Δt) between the wave fronts of the incident and transmitted waves and making use of expression (4.45).

$$\sqrt{\alpha_\infty} = \frac{c_0\Delta t - d_m}{h} \quad (4.46)$$

where, $d_m = 6.35 \times 10^{-3} \text{ m}$ is the diameter of the 1/4'' microphone and h is the sample thickness. The method is capable of measuring the tortuosity with a relatively high accuracy of 4-5%.

An alternative method (the n^2 -method) has been proposed by Leclaire et al (1996) and is based on the measurement of the high-frequency behaviour of the real part of the complex wavenumber in a porous medium. It is possible to demonstrate that at high frequencies of sound (λ_V) the refraction index is an asymptotic function of $\omega^{-1/2}$, i.e.

$$n = \frac{\text{Re}k_b}{\omega/c} \cong \sqrt{\alpha_\infty} \left(1 + A\omega^{-\frac{1}{2}} \right), \omega \rightarrow \infty \quad (4.47)$$

where A is some parameter which is frequency-independent, but relates to the pore geometry, internal pore surface area and physical properties of the filling fluid (e.g. air). A typical behaviour of equation (4.47) is shown in Figure 4.20. This figure presents the measured and interpolated data for the refraction index in a loose granular mix of keramsite with characteristic particle dimension of 2.2mm. The point of intercept on the graph in Figure 4.20 is the sought value of tortuosity, $\sqrt{\alpha_\infty} \cong 1.62$. Unlike the method of ultrasonic time of flight, the n^2 -method does not require ultrasonic data on the sound speed in the porous sample. In the above example, the data presented in Figure 4.21 is plotted in the frequency range of 280 - 5096 Hz and the accuracy of the method is mainly limited by the ability of the system to measure complex wavenumber in the sample and by the slope gradient A .

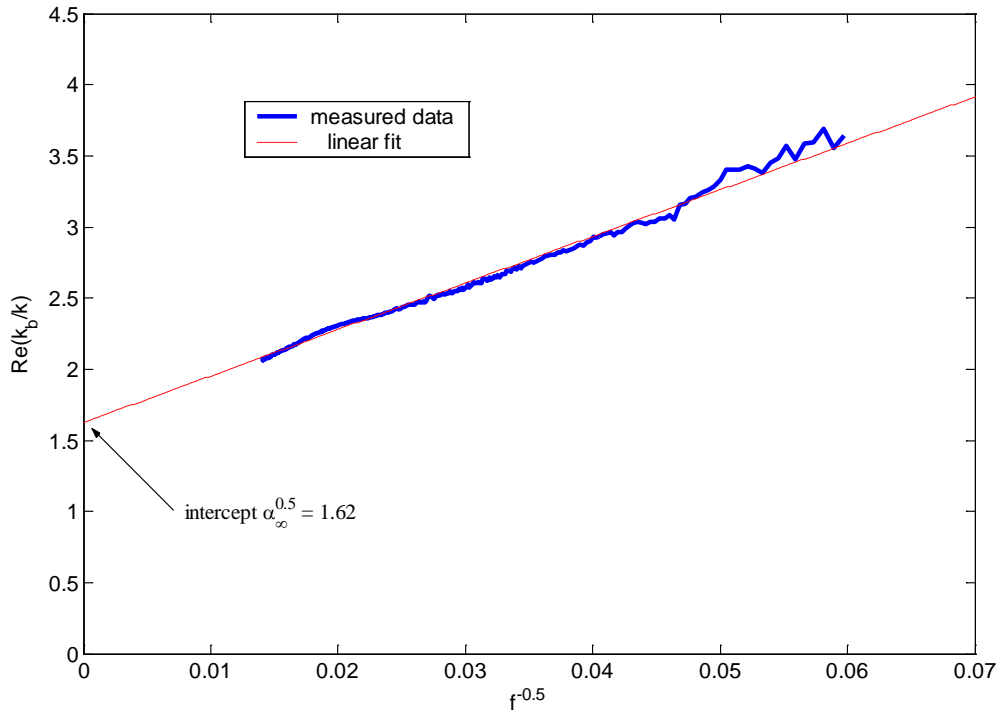


Figure 4.20: Determination of the tortuosity using the n^2 -method

Another simple method of determining tortuosity from measured data on the characteristic impedance was proposed by Voronina and Horoshenkov (2003). The method is based on the observation that above a certain critical frequency $f \geq f_{cr}$ (f_{cr} is equivalent to the Biot frequency, f_v) the behaviour of the real part of the characteristic impedance is asymptotic $Re z_b \cong \sqrt{\alpha_\infty / \phi}$. This typically occurs in porous media with a relatively low flow resistivity and medium/high values of porosity. In the case of loose granular media the value of the critical frequency can be determined semi-empirically and relates to the material porosity, tortuosity and the particle size (D), i.e.

$$f_{cr} = \frac{200\eta(1-\phi)^2(1+\phi)^4}{\pi D^2 \rho_0 (\sqrt{\alpha_\infty - \phi})^2} \quad (4.48)$$

In the case of other types of porous media, e.g. those composed of fibres or mixed fibres and grains, the critical frequency cannot be predicted by the above expression and should be taken as $f_{cr} = f_v$. Figure 3.15 presents the data for the behaviour of the real part of the acoustic characteristic impedance ($W_a = Re z_b$) of three loose granular materials with progressively increasing flow resistivity and decreasing characteristic particle dimension.

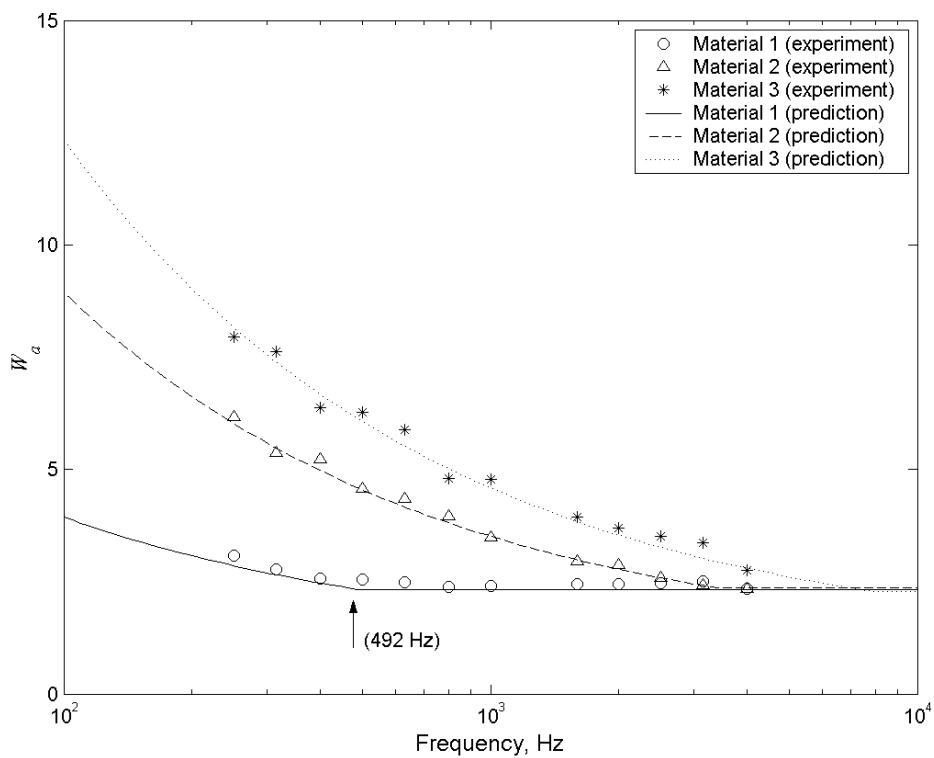


Figure 4.21: Determination of tortuosity from the asymptotic behaviour of the real part of the characteristic impedance

The results show that in the case of material 1 (loose vermiculite) the characteristic frequency is low ($f_{cr} = 492 \text{ Hz}$) because of the relatively large grain size ($D = 1.4 \text{ mm}$). Above the characteristic frequency the behaviour of the characteristic

impedance is almost frequency independent and $W_a = \sqrt{\alpha_\infty}/\phi \cong 2.3$. Since the porosity is easily measurable by other non-acoustic means (see section 3.3.1) the tortuosity can be deduced from $\sqrt{\alpha_\infty} \cong 2.3\phi$.

4.15 Thermal conductivity

Low thermal conductivity is a common property of porous materials like foams and fibres. One of the first instruments developed for studying thermally insulating materials was developed by Lees (1898). The method was improved by Poensgen (1901), further modifications to the method have been made, and many of the new techniques have been incorporated into the international standard ISO 8302:1991. This standard is an embodiment of the best practices contained in many of the national standards that were available at the time. The basic principle of the guarded hot plate method is to generate a known unidirectional heat flux through the specimens so that they appear as slabs of infinite width bounded by parallel planes. To achieve these aims, it is customary to use a heater plate comprising two parts, surrounded by an annular guard and separated from it by a small air gap, which acts as a thermal barrier. Heat flows from the heater plate through the specimen to cold plate maintained at a stable lower temperature.

The method described in BS 1902-5.8 is based on the split column principle for mean temperature in the range 300°C to 850°C, this method was adapted to measure thermal conductivities for temperatures in the range of 75-150°C. The main differences are the material used for the blocks, as suggested in BS 1902-5.8 the steel blocks have been replaced with two aluminium cylinders in order to increase the thermal conductivity and the heat flux to and from the test sample at a lower temperature. Also it was impractical

to use a thermocouple pair inserted in the sample instead a pair of thermocouples installed in the top and bottom blocks were used to determine the temperature difference (Figure 4.22).

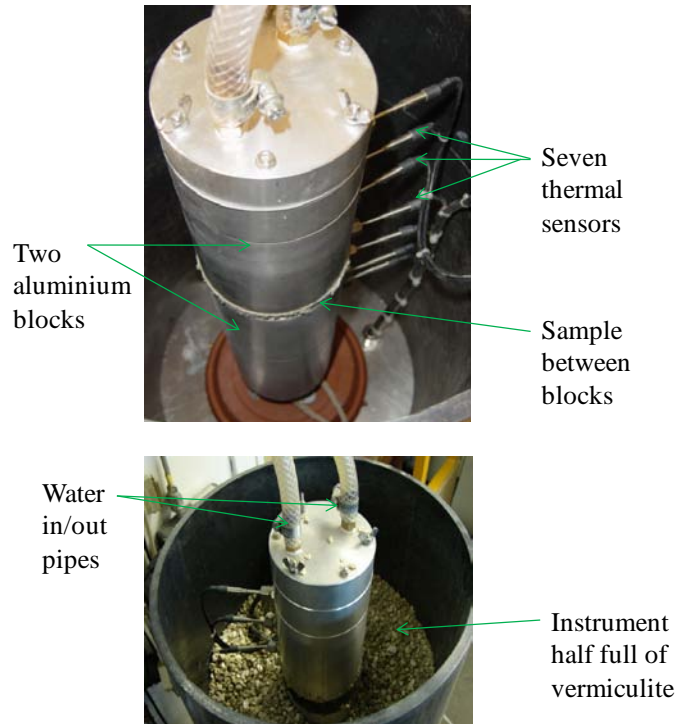


Figure 4.22: Thermal conductivity apparatus setup

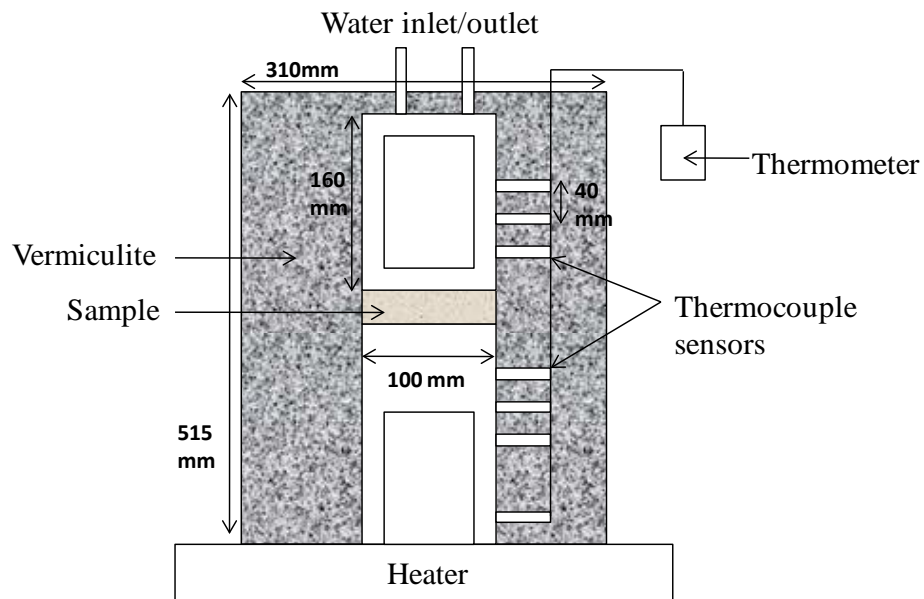


Figure 4.23: Schematic diagram of the thermal conductivity apparatus

Using this adopted instrument the thermal conductivity, $\lambda_t (W/(m.K))$ was deduced from the power supplied, Q_t , the mean difference in temperature between the plates, $T_n - T_c$, the cross sectional area of the blocks, A , and the mean thickness of the specimen, l , using an equation originally developed by Fourier for conduction of heat in one dimension,

$$\lambda_t = \frac{Q_t l}{A(T_n - T_c)} \quad (4.49)$$

The resistance R can be calculated by using,

$$R = \frac{d}{k} \quad (4.50)$$

The thermal transmittance U value ($W/(m^2.K)$) is the inverse of the R value and d is the sample thickness in meters.

$$U = \frac{1}{R} \quad (4.51)$$

The lower the U value the better the performance of the material for thermal transmittance.

4.16 Rate of reaction of binder with water

The rate of reaction is defined as how fast a reaction takes place. For a chemical reaction the rate equation links the rate of a reaction to the concentration of each reactant. It is of the kind,



$$r = k_r [A]^{n'} [B]^{m'} \quad (4.53)$$

where A and B are reactants and $C + D$ are the products, the rate of reaction is defined as the rate at which the reactant concentration decreases over time.

$$\text{Rate of reaction } (k_r) = \frac{\Delta c}{\Delta t} \quad (4.54)$$

where Δc is the change in concentration of reactants and Δt is the change in time.

$$\text{Rate of reaction } (k_r) = -\frac{\Delta[AB]}{\Delta t} \quad (4.55)$$

The minus sign signifies that the concentration of A and B falls over time, and the plus sign signifies that the concentration of AB increases over time. Figure 3.18 shows the apparatus used to measure the rate of reaction.

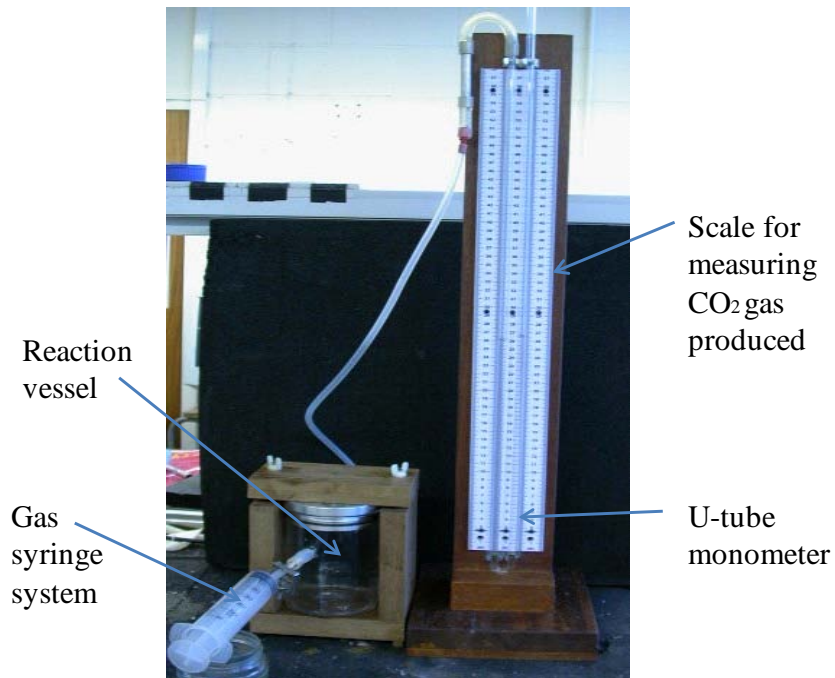


Figure 4.24: Rate of reaction apparatus setup

The reaction was carried out in the reaction vessel shown in Figure 4.24, the CO₂ gas produced during the reaction of MDI binder with water displaces the water level in the U tube monometer; the water displaced in the monometer is directly proportional to the amount of CO₂ gas produced during the reaction. The readings were taken by withdrawing the syringe and levelling the two meniscuses. The rate of a chemical reaction is affected by the following factors, the concentration of reactants, temperature, and catalyst. For a faster reaction the k_r value is high, whereas for a slower reaction the k_r will be low.

Three different types of porous samples were produced by the reaction of water with binder (Figure 4.25) samples with broad pore size distribution, double porosity materials (porous material containing two different scales of pores), and mono-porous samples. In a typical porous material for acoustic applications the pores are angular and irregular in cross section, pore sizes range from hundredth of a micrometer up to macro-pores that are between two to eight centimetres. The pore size is highly variable from point to point within the material also the pores have a high level of interconnectivity. Figure 4.26 shows images of two samples with different pore size distributions taken using an electron microscope. From such images, the level of connectivity, shape variation, size, and curvature of real pore structures is apparent.

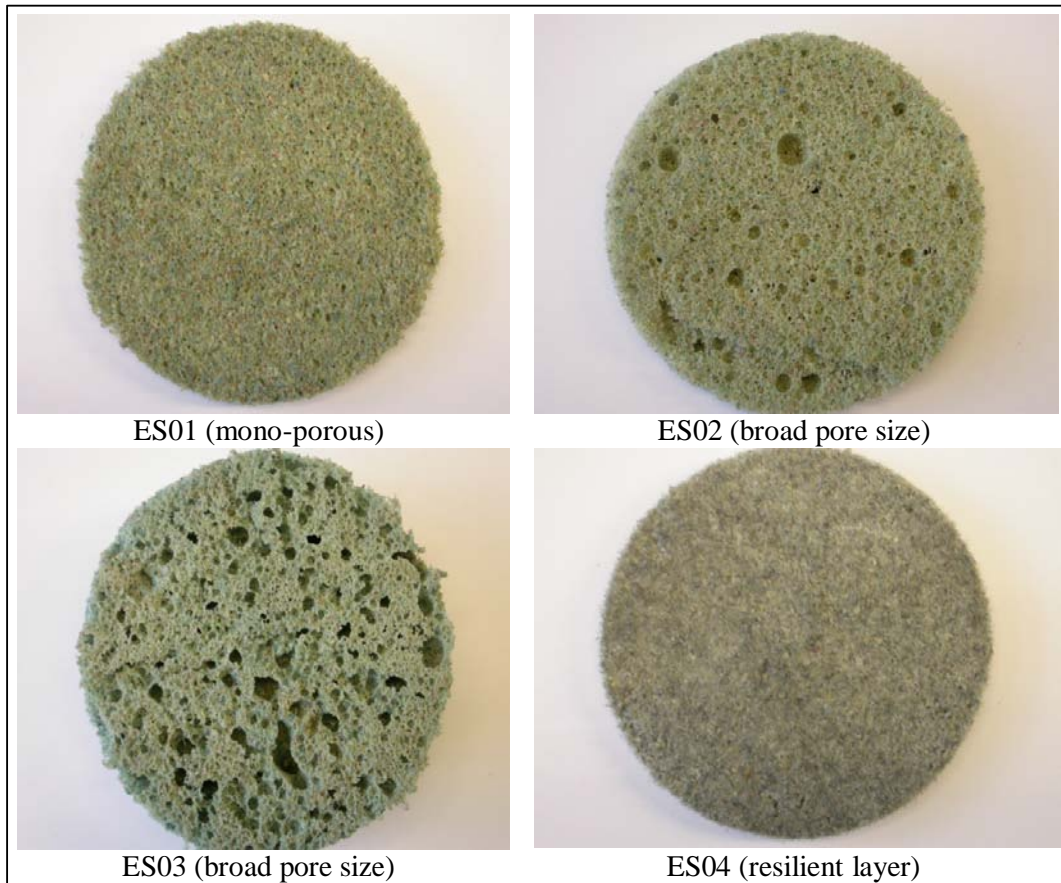


Figure 4.25: Photographs of four types of materials produced using the cold extrusion process

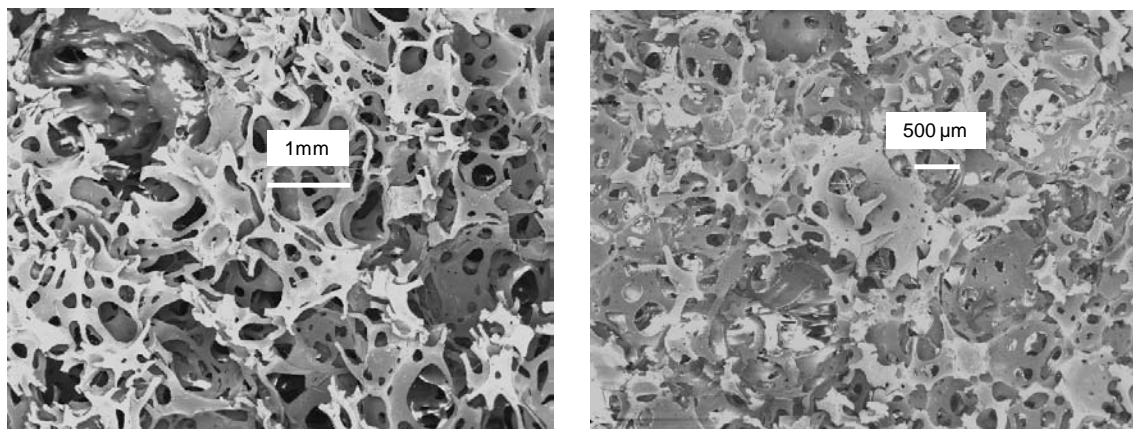


Figure 4.26: Scanning electron micrographs of materials with a broad pore size distribution (left) and narrow pore size distribution (right)

4.17 Determination of the accuracy of the acoustic instruments (round robin test)

Characterisation of porous media is now a relatively routine procedure which is carried out in many laboratories worldwide to determine the acoustical absorption performance of these materials or to deduce the fundamental non-acoustical data related to their porous microstructure. A standard technique to characterize these materials is the impedance tube method (see section 4.8) which typically allows one to measure the surface impedance and absorption coefficient of relatively small (e.g. 29-100 mm) samples of porous media. This data can then be used to deduce some of the non-acoustical parameters of porous materials which link to their pore geometry and proportion of open, interconnected pores. As a result, the characterisation process relies heavily on the accuracy of experimental data on the acoustic surface impedance or absorption coefficient. The accuracy of this technique is affected by the quality and homogeneity of the material samples, their environmental and operational conditions during the experiment, the quality of the setup, and the signal processing method. These conditions and measurement apparatus can vary from laboratory to laboratory and their effect on the measured values of the sound absorption coefficient is largely unknown.

A majority of the relevant studies have been carried out in individual laboratories and the author is not aware of any works offering systematic experimental data on the performance of the impedance tube method between individual laboratories (i.e. inter-laboratory data) for a particular set of material samples. These data should be obtained using independent sample preparation techniques, impedance tubes of different diameters, different excitation stimuli, and signal processing methods. A majority of previous works focused on the acoustical properties of highly porous, light-weight

foams and glasswool. As a result, there is a lack of data on the reproducibility of the standard impedance tube experiment on material samples made from granular-like media for which a limited porosity and a relatively low flow resistivity are characteristic.

In order to determine the accuracy of the acoustic data presented in this chapter using the standing wave tube method discussed in section 4.8, the absorption coefficient data obtained for different samples of the same sheet of material in the same laboratory will be compared between different laboratories around the world.

In total seven acoustic research centres were involved in this work. These were:

1. University of Perugia (Italy),
2. Katholieke Universiteit Leuven (Belgium),
3. ENTPE (Lyon, France),
4. Gesellschaft für Akustikforschung (Dresden, Germany),
5. University of Bradford (UK),
6. University of Ferrara (Italy)
7. Sherbrooke University (Canada).

The results for three porous media of different classes, reconstituted porous rubber, reticulated foam, and fibreglass will be presented. These materials were chosen to cover the range from relatively low ($10 \text{ kPa}\cdot\text{s}\cdot\text{m}^{-2}$) to relatively high ($140 \text{ kPa}\cdot\text{s}\cdot\text{m}^{-2}$) flow resistivity and to be representative of typical, commercially available acoustic porous materials. Table 4.3 provides a summary of some physical and geometrical characteristics of these materials. The values of parameters presented in this table were

averaged over all the range of data provided by all the partners for all the material specimens studied in this round robin test. This table also presents the standard deviation for the measured flow resistivity and porosity data.

Table 4.3: A summary of the averaged characteristics of the investigated porous materials

Material	Description	Mean porosity	Mean flow resistivity, (kPa s m⁻²)	Mean density, (kg/m³)	Mean thickness, (m)
A	reconstituted porous rubber	0.80±0.02	141.4±44.0	242.0	0.0245
B	Reticulated foam	0.98±0.01	9.9±0.8	8.8	0.0197
C	fibreglass	0.97±0.03	11.7±1.9	21.0	0.0290

Each partner was provided with a 400 mm x 400 mm sheet of the above materials. Specimens of these materials have been cut individually by the partners using a circular cutting tool or water jet cutting machine to fit the diameter of the standing wave tube. The diameter of the standing wave tube, the measurement method, the sample preparation procedure, and the mounting method for the sample used by the partners are detailed in Table 4.4. The measured properties were the surface impedance z_s and the absorption coefficient (α) of the material sample backed by a rigid wall, i.e.

$$z_s = z_b \coth(-ik_b h) \quad \text{and} \quad \alpha = 1 - \left| \frac{z_s - \rho_0 c}{z_s + \rho_0 c} \right|^2 \quad (4.56)$$

Here z_b is the characteristic impedance, k_b is the wavenumber within the material, and h denotes the material thickness.

Table 4.4: Equipment and sample preparation procedures (HM – home made tube; H – horizontally installed tube; V – vertically installed tube)

Partner	Tube diameter, (m)	Tube length/microphone spacing, (m)	Material preparation method
i.	44mm/HM/V	1m/0.03m	water jet/circular tool
ii.	46mm/HM/H	1.32m/0.02m	rotating blade
iii.	38mm/HM/H	1m/0.02;0.03;0.05m	rotating blade
iv.	29mm/BK4206/H	0.4225m/0.02m	rotating blade
v.	29mm/BK4206/H	0.4225m/0.02m	rotating blade
vi.	29mm/HM/H	0.4225m/0.02m	rotating blade
vii.	45mm/HM/H	0.37m/0.025m	water jet

The partners used a range of commercially available impedance tube apparatus and impedance tubes specially designed and constructed for their laboratories. All the microphones used in these experiments were standard measurement 1/4” microphones. Six out of seven partners used identical or similar types of microphones provided by Brüel and Kjær. Partner 6 used specialised 1/4” microphones supplied by Microtech Gefell. The type of acoustic stimulus was mainly restricted to random noise. Partners 1, 2, and 7 used maximum length or phase-modulated random noise sequences. The numbers of averages were adapted to the type of the acoustic stimulus and the signal-to-noise ratio observed during the experiments. This number varied from 8 inches in the case of the maximum length sequences to 100 inches in the case of random noise. The type of the electronic hardware used for data acquisition varied from a specially dedicated commercially available Brüel and Kjær PULSE system (partners 5 and 6), general purpose A/D analyzers (partners 2 and 3), and high-quality sound cards (partners 1 and 4). Each impedance tube was driven by a single loudspeaker which was

adapted to the size and the frequency range of the impedance tube (typically in the range of 100-6000 Hz). It was assumed that the non-linearity in the speaker response and tube vibration effect could be neglected. The sampling frequency and the sequence length used in the Fourier analysis were chosen so that to cover the desired frequency range and provide adequate frequency resolution in the transfer function spectrum as suggested in ISO 10534-2 (1998). The equipment was properly calibrated prior to the start of the experiments to compensate for the microphone channel mismatch using the procedure suggested in 10534-2 (1998) for those partners who used two independent microphone channels. The effects of temperature and atmospheric pressure variations were compensated as suggested in 10534-2 (1998). The material thickness was measured to ± 0.1 mm using a set of calibrated callipers.

The results for the acoustic surface impedance obtained for Material A indicate that the dispersion in both the real and imaginary part is considerable. Specifically, the maximum dispersion in the real part of the impedance is ± 31 % in the frequency range below 1000 Hz. The dispersion in the imaginary part of the impedance in this frequency range is limited and increases with the increasing frequency. This phenomenon is consistent in the results obtained in other laboratories as indicated in Figure 4.26. Reconstituted porous rubber is a highly resistive material and the dispersion is likely to be attributed to dispersion in the values of the flow resistivity of the investigated material samples. The standard deviation in the measured values of the flow resistivity obtained for this material using the direct measurement is relatively high and compares well with that observed in the measured data for the real part of the surface impedance ($\Delta\sigma = 31$ % vs. $\Delta\text{Re } z_s = 31$ %). This effect is expected and explained by the dominant $\sigma/3$ term in the expression 4.57.

$$z_s \approx \frac{\sigma}{3} + \frac{i}{\phi\gamma kh}, \quad k \rightarrow 0 \quad (4.57)$$

where, k is the wavenumber in air, γ is the ratio of specific heats and ϕ is the material porosity.

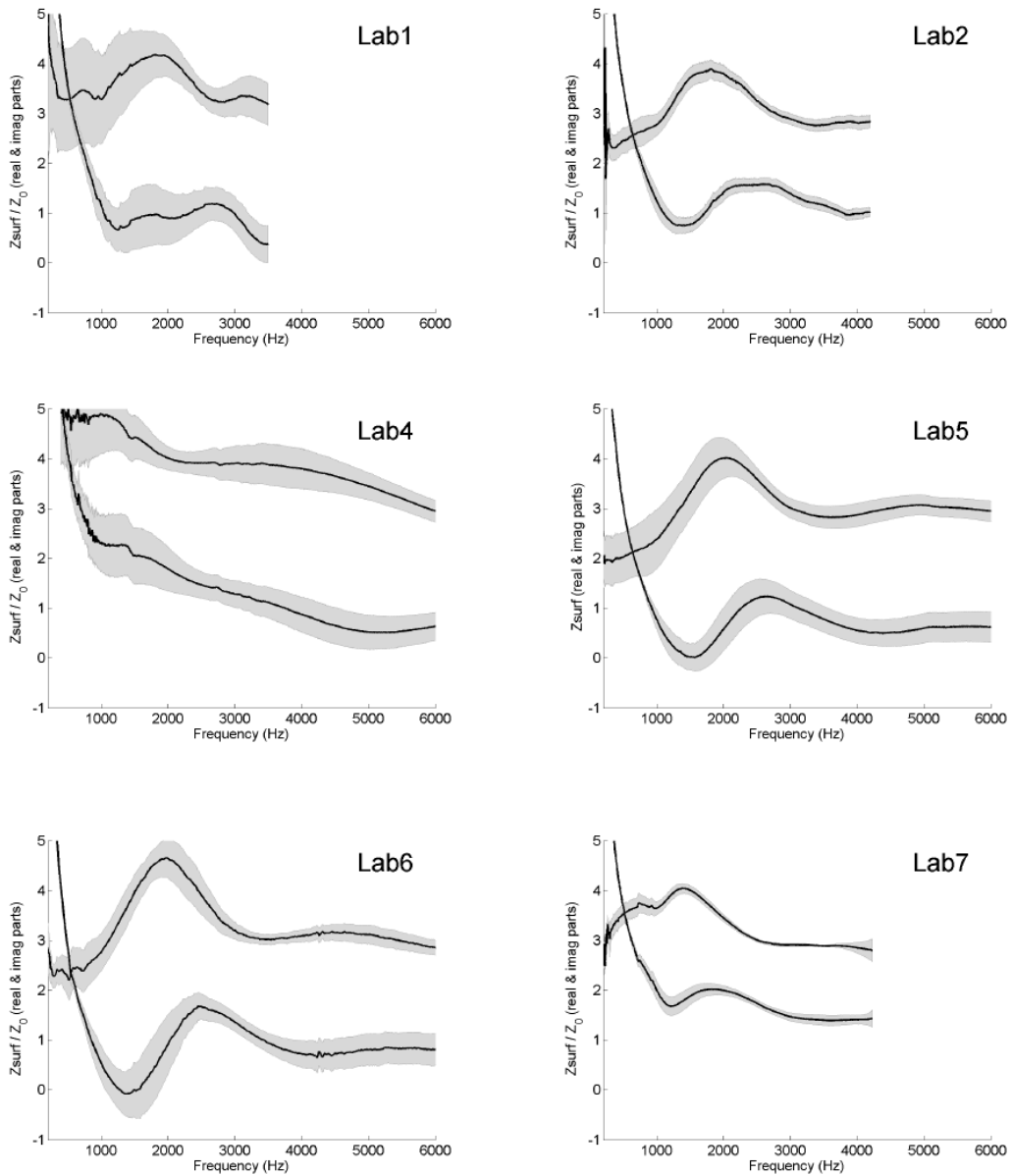


Figure 4.27: Individual results of the measurements of the real and imaginary part of the normalised surface impedance for Material A for all partners

The inter-laboratory examination suggests that there is a similarity in the behaviour of the mean impedance between laboratories 1, 2, and 7 but there are noticeable differences in the dispersion. These laboratories used the impedance tubes of similar diameter (44–46 mm) and similar type of acoustic excitation. The maximum dispersion in these results is observed in the case of laboratory 1 and the minimum is in the case of Laboratory 7. This is likely to be attributable to the quality of the sample mounting conditions and the number of tested specimens. The behaviour of the results from laboratories 5 and 6 is comparable both in terms of the dispersion and mean values of the acoustic surface impedance. These two laboratories used identical types of impedance tubes (Brüel and Kjær 4206), signal analysis hardware (Brüel and Kjær PULSE) and the same software setup.

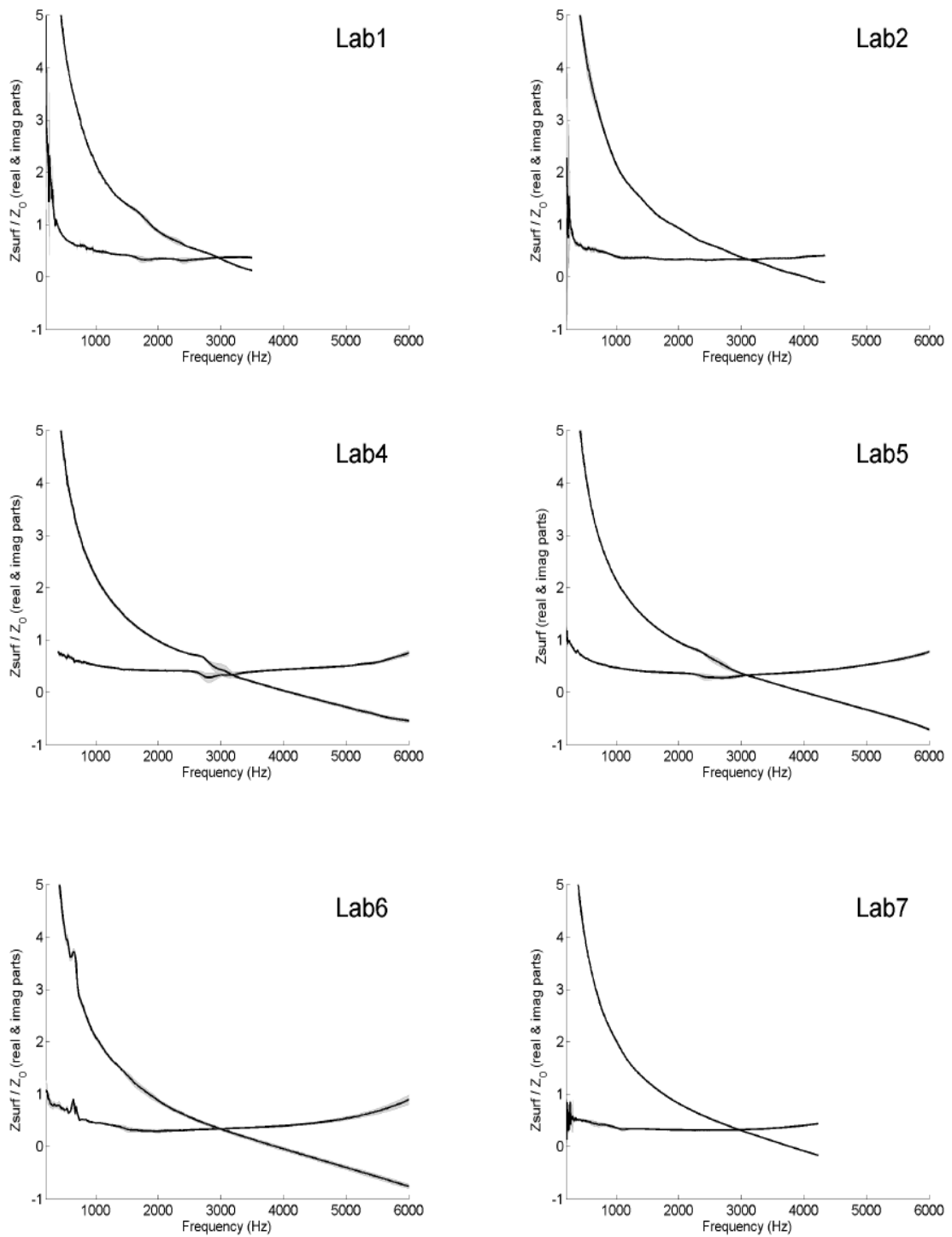


Figure 4.28: Individual results of the measurements of the real and imaginary part of the normalised surface impedance for material B for all partners

The behaviour of the impedance data obtained in Laboratory 4 differs from that obtained in the other laboratories, but the level of dispersion is similar to that observed in the results from laboratories 5 and 6. These three laboratories use the identical impedance tubes but laboratory 4 uses a specialised sound card instead of a PULSE analyser (Table 4.5).

Table 4.5: Summary of the acoustic stimuli and the hardware used in the round-robin experiments (MLS – maximum length sequence; PRN – pseudo-random noise; RN – random noise; WN - “white” noise)

Partner	Type of acoustic stimulus	Number of averages	Electronic hardware	Microphone type
i.	MLS	8	Marc-8 sound card	BK4187
ii.	PRN	16	NI card PXI-4461	BK4187
iii.	RN	30	HP-35060A analyser	BK4135
iv.	WN	100	VX-Pocket PCMCIA	BK4187
v.	RN	100	BK PULSE	BK4187
vi.	RN	100	BK PULSE	Microtech Gefell Type M360
vii.	PRN	6	MNS Tube-X	BK4187

The results show that the dispersion of the acoustic absorption spectra for material B is considerably less (<10% except around the frame resonance Figure 4.31) than that in the case of material A which relates to the consistent air flow resistivity values and the constant material thickness. The largest values of the standard deviation, reaching locally more than 30% for Laboratory 4, occur near the structural resonance in the material frame which frequency depends on the mounting conditions attained during the

measurement. It is clear from the results obtained in Laboratory 2 and 7 that the selected mounting conditions using the appropriate sample constraints enabled to move the structural resonance frequency out of the measurement spectral range.

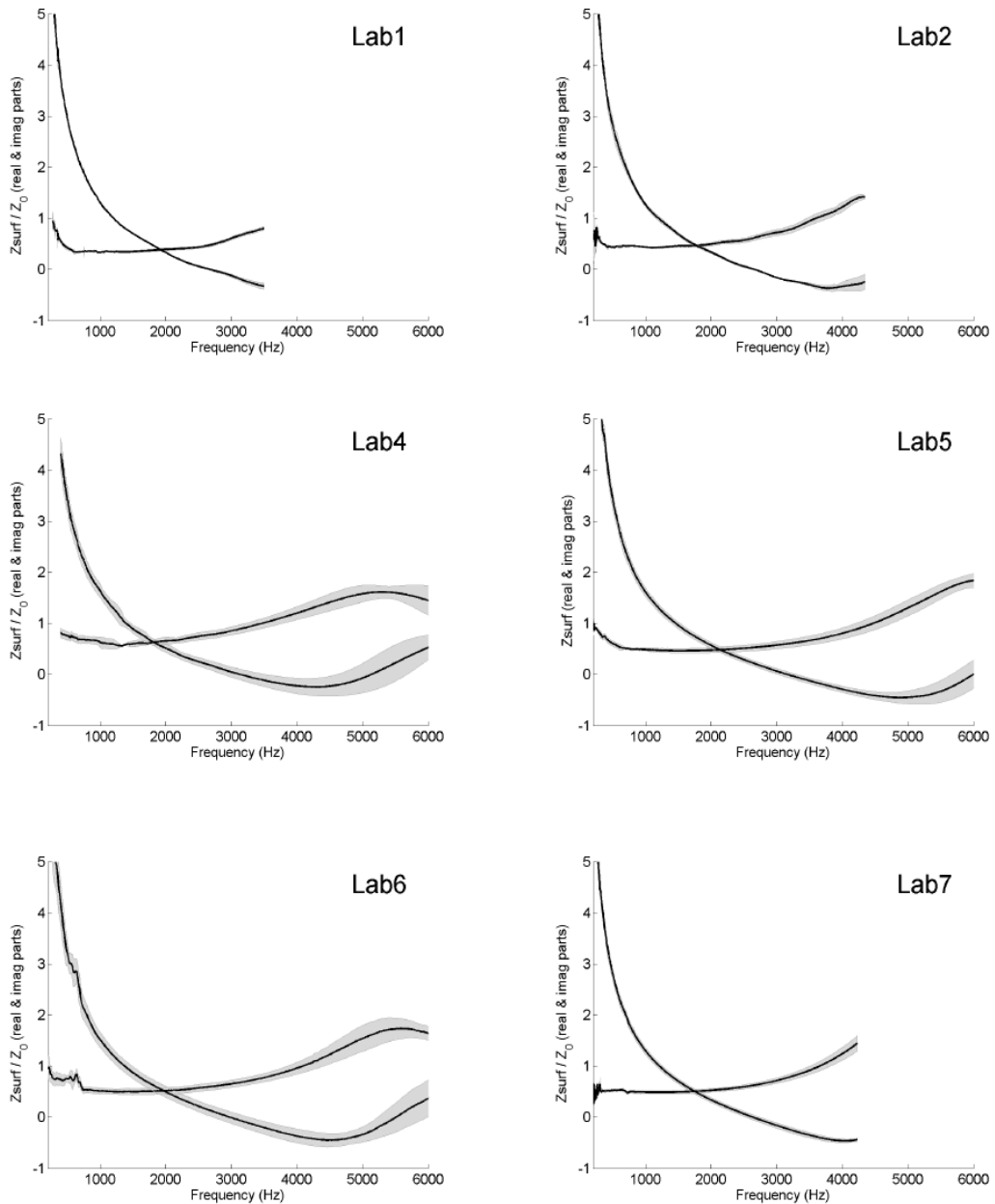


Figure 4.29: Individual results of the measurements of the real and imaginary part of the normalised surface impedance for Material C for all partners

The density of material C is approximately 2.5 times greater than that of material B and the material exhibits a relatively low bulk modulus of approximately 100 kPa. The latter characteristics seem to drive the resonance frequency towards the lower spectral end so that none of the presented results show the distinctive frame resonant behaviour. Figures 4.30 - 4.32 present the measured data for the real and imaginary parts of surface impedance together with their standard deviation obtained by each partner for materials labelled A, B, and C, respectively.

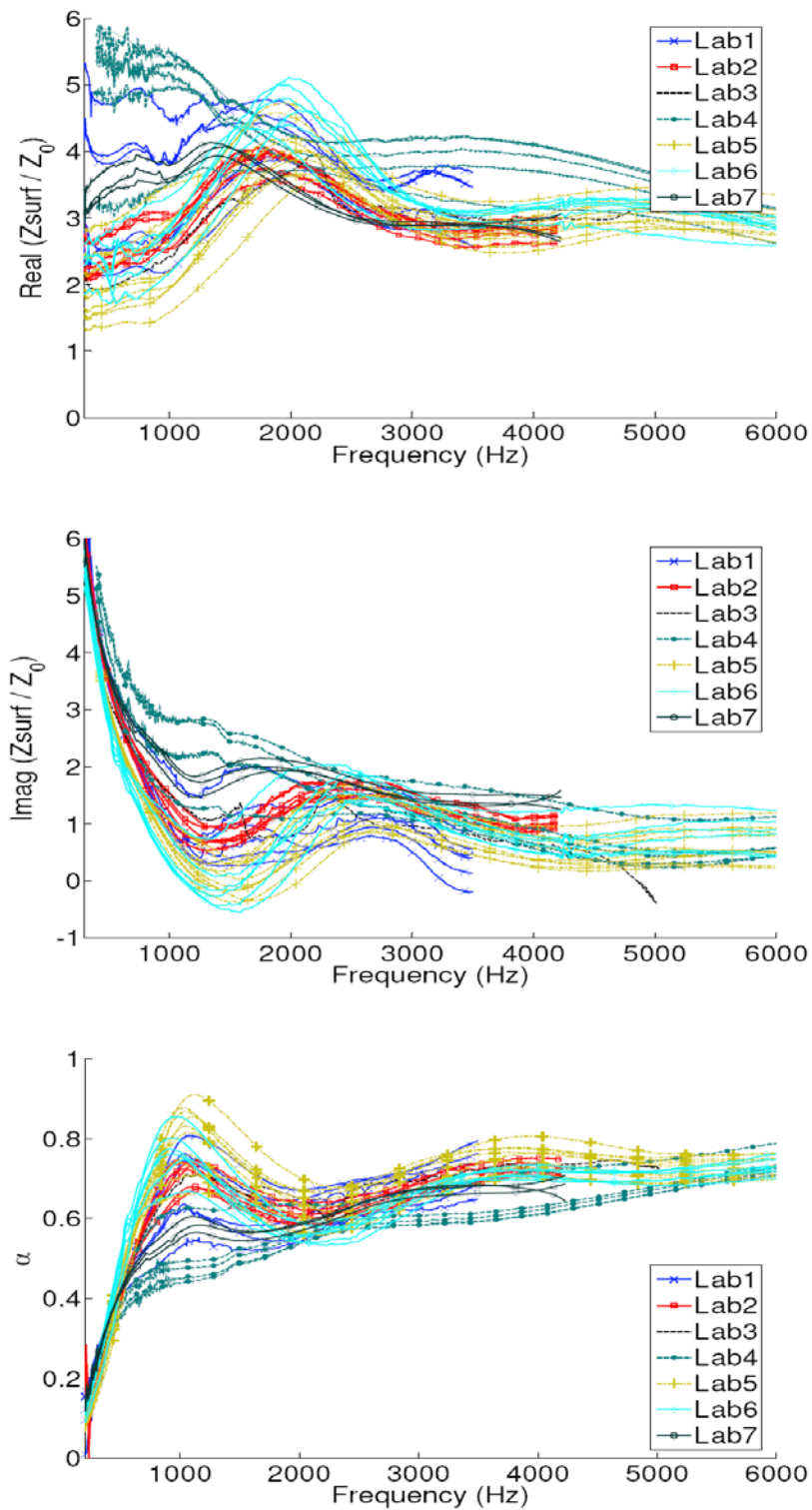


Figure 4.30: (colour online) Inter-laboratory measurements of the real part (top), imaginary part (middle) and the sound absorption coefficient (bottom) for Material A

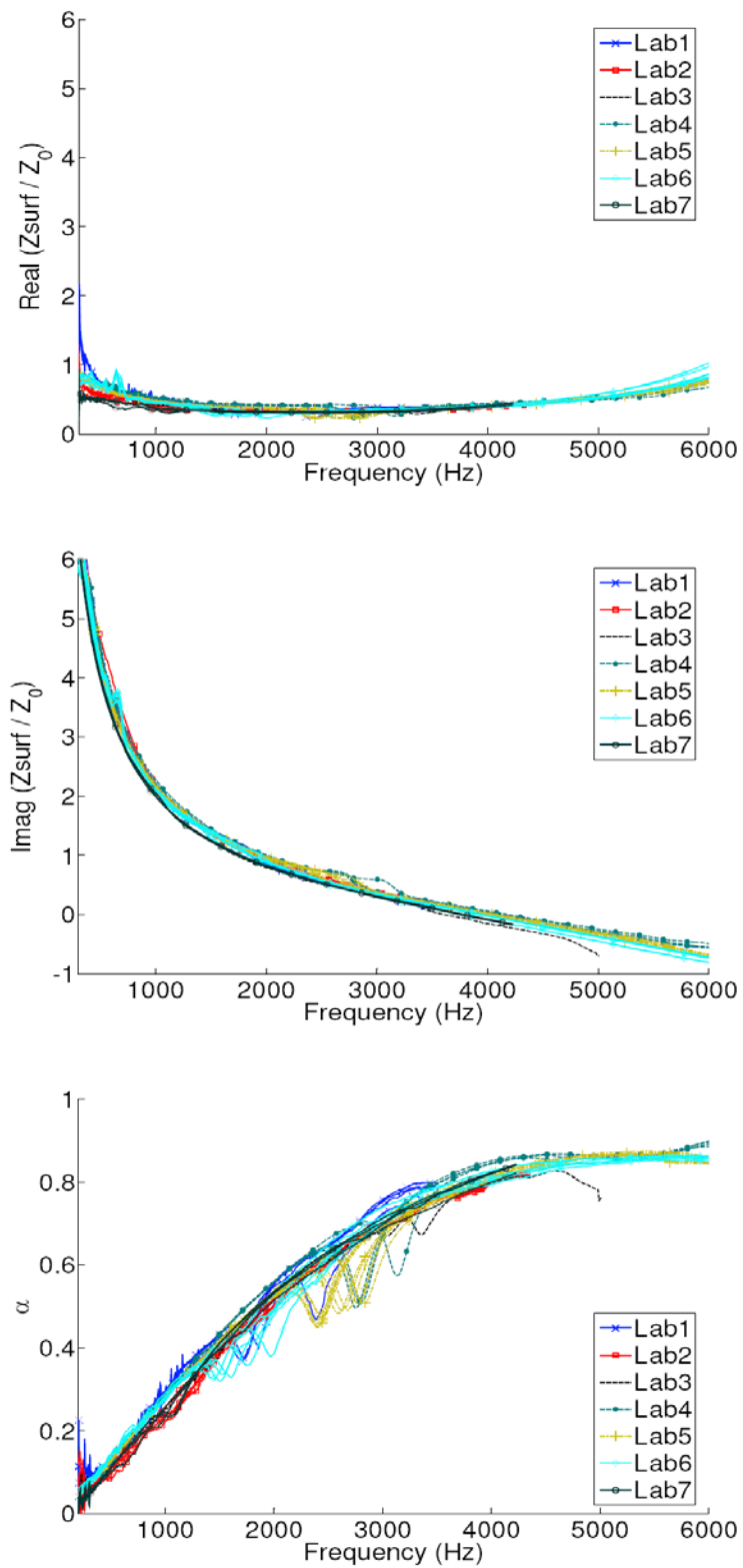


Figure 4.31: (colour online) Inter-laboratory measurements of the real part (top), imaginary part (middle) and the sound absorption coefficient (bottom) for Material B

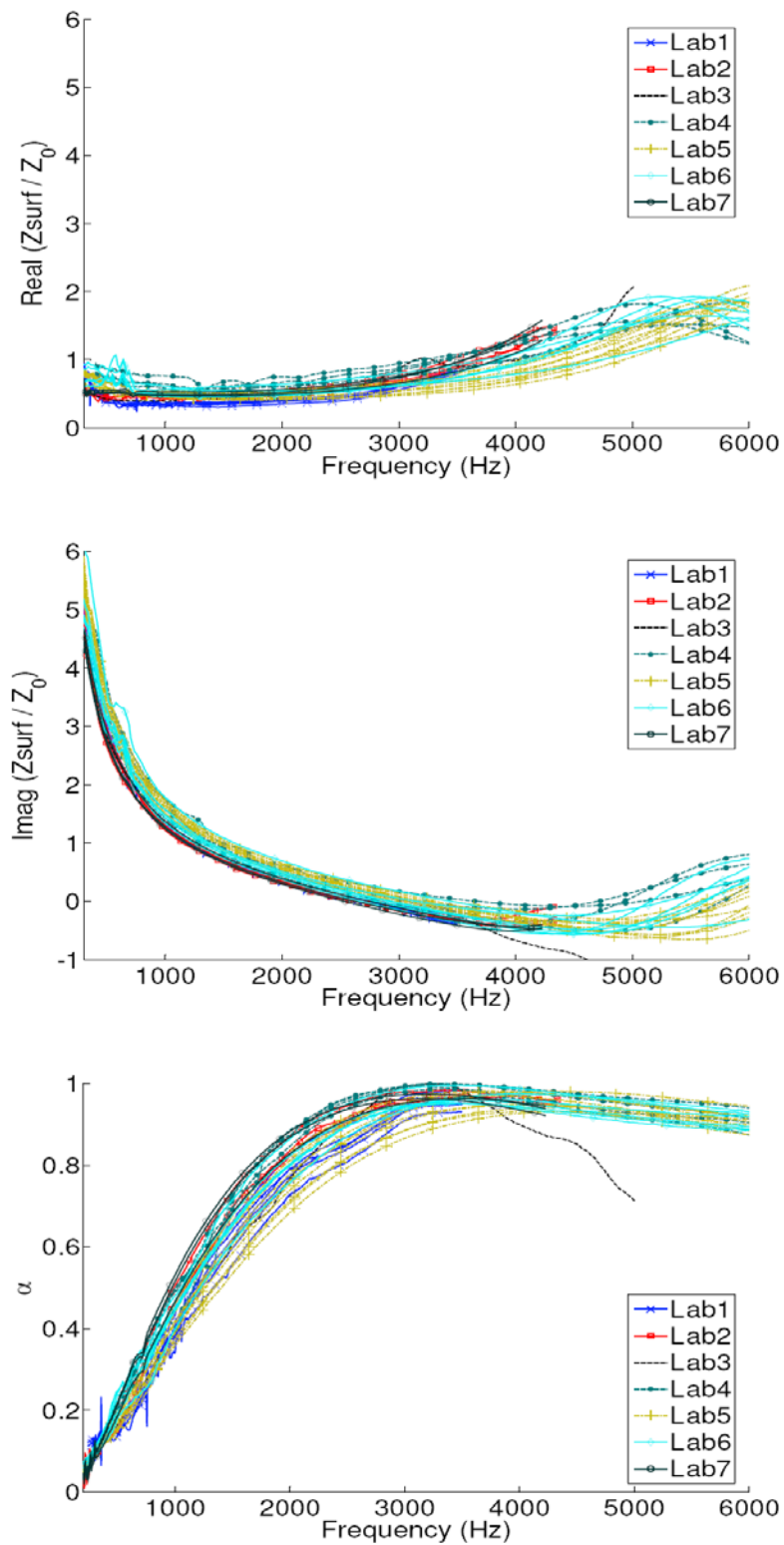


Figure 4.32: (colour online) Inter-laboratory measurements of the real part (top), imaginary part (middle) and the sound absorption coefficient (bottom) for Material C

The high flow resistivity and the acoustic penetration depth, $\text{Re}(1/k_b)$ in these materials are rather sensitive to the fluctuation of the material air resistance and the mounting conditions. The latter is likely to affect the thickness of the circumferential air gap and the compression rate of the investigated sample. These effects are reflected in the position and amplitude of the first interference maxima and minima in the absorption coefficient spectra which can disappear completely due to the low value of the penetration depth (e.g. data from laboratory 4).

Inter-laboratory standing wave tube measurements have been performed on samples of three commercial porous products which represent low and high permeability porous media. One standard method of testing has been used, namely the ISO 10534-2 (2001). The maximum dispersion in the measured spectra for the surface impedance (5-6 fold) and acoustic absorption coefficient (2 fold) has been observed in the results between individual samples and individual laboratories in the case of low permeability, low homogeneity, broad pore size distribution, reconstituted porous rubber (material A). The least dispersion (<20 %) in the data was observed in the case of high permeability porous foam (material B). This material is consistent in terms of its thickness and air flow resistivity values. Laboratories 2 and 7 demonstrated that it is possible to use the appropriate sample constraints to move the structural resonance frequency out of the measurement spectral range to minimise the dispersion in the measured acoustical data (see Figure 4.28).

It is suggested that the existing ISO10534-2 (2001) should be revised to define more precisely: (i) the procedure for sample preparation and minimum number of tested specimen; (ii) the minimum size of the sample as a function of the material density, bulk modulus of the material skeleton and flow resistivity; (iii) the sample mounting

conditions (iv) the type of stimuli and signal processing method, (v) procedure for merging material data obtained in tubes of different diameters, procedure which has not been discussed here. The revised standard procedure should enable quantification of the intrinsic experimental errors.

4.18 Summary

In this chapter a comparison of different modelling approaches for highly heterogeneous porous media has been carried out. Several characterisation methods used to study the acoustic materials have been discussed. The accuracy of the acoustic and key non-acoustic characterisation methods were determined through an inter-laboratory experiment (round robin test). The purpose of this work was to determine how reproducible the standard impedance tube data was for samples made from granular like media for which a limited porosity and a relatively low flow resistivity are characteristic.